7. S18Y polymorphism in UCH-L1 and PD

A polymorphism in UCH-L1 resulting in the amino acid substitution of serine 18 to tyrosine was first reported in 1999 with the possible protective effect against PD (Maraganore et al., 1999). This polymorphism is relatively common in Japanese (allele frequency is 39–54%) and Chinese (~50%) populations, but is rare in European (14–20%) populations (Liu et al., 2002). Further analysis indicated that this inverse association between this polymorphism and PD exists in some populations, such as in Japanese and Chinese but not in others (Maraganore et al., 1999; Mellick and Silburn, 2000; Wintermeyer et al., 2000; Levecque et al., 2001; Wang et al., 2002; Elbaz et al., 2003; Toda et al., 2003; Maraganore et al., 2004; Facheris et al., 2005; Healy et al., 2006; Tan et al., 2006; Carmine Belin et al., 2007). This association was most apparent for younger cases of PD compared with younger controls. In addition, the protection was dependent on the S18Y allele dosage.

A group showed that the Ub ligase activity of UCH-L1, as mentioned above, is responsible for this reduced risk for PD associated with the S18Y polymorphism (Liu et al., 2002). Ub ligase activity of UCH-L1 was shown towards α-synuclein (probably di-ubiquitinated α-synuclein) as a substrate, leading to Ub chain formation (elongation) through lysine 63 of the Ub molecules (Fig. 1). When substrates are poly-ubiquitinated via lysine 63 of Ub, they escape from Ub-proteasomal system (UPS)-dependent protein degradation leading to the stabilization of the substrate. UCH-L1^{WT} tended to form dimers in contrast to UCH-L1^{S18Y,} leading to increased ligase activity in UCH-L1^{WT} (Table 1). Thus, the stability of α-synuclein may be enhanced in the presence of UCH-L1^{WT} compared to UCH-L1^{S18Y}. This difference may reduce the protein level of α-synuclein and reduce the risk of PD in subjects with the S18Y polymorphism. From these experiments, the authors proposed a mechanism in which the ligase activity of UCH-L1 might affect the morbidity of PD in the brain.

Using small angle neutron scattering (SANS), we compared the structural differences that exist between UCH-L1 variants, wild type, I93M and S18Y in aqueous solution (Naito et al., 2006). SANS is an effective method to analyze detailed protein configuration in solution. Using this method, all of the recombinant UCH-L1 variants formed dimers in water. I93M was more ellipsoidal compared with wild-type protein, and S18Y promoted globularity compared with wild-type protein (Table 1). Thus, the shape of the mutant UCH-L1 in water correlated with the risk of PD. Although further analysis should be performed to determine the significance of UCH-L1 dimerization and the S18Y polymorphism for neurodegeneration, the experiments performed in these two laboratories have provided some clues.

8. Concluding remarks and future prospects

UCH-L1 is indicated as a multi-functional protein (Fig. 1) with abundant expression in neurons. In addition, it has become apparent that UCH-L1 may contribute to the pathogenesis of PD and AD. Thus, it is a probable diagnostic and medicinal target of these diseases. However, the mechanism of neurodegeneration induced by I93M mutation and the mechanisms underlying the decreased expression, amino-terminal truncation and increased oxidative modification of UCH-L1 in neurodegenerative diseases have yet to be revealed. In addition, there are several unresolved issues regarding the molecular functions and regulation of UCH-L1. The *in vivo* substrates need to be defined. The ways in which the function and localization of UCH-L1 are regulated are largely unknown. The identification and the analysis of the interacting partners might give us some clues, one of which is Jun activation domain binding protein (JAB1) in H1299 cell, a lung cancer cell line (Fig. 1) (Caballero et al., 2002), though their interaction in the brain is unknown. Recently, a physiological function of an isozyme UCH-L3 was identified in the oxidative stress-induced apoptosis of photoreceptor cells, neurons that reside in the retina (Semenova et al., 2003; Sano et al., 2006). In addition, a reciprocal function of UCH-L1 and UCH-L3 has been proposed in the heat stress-induced apoptosis of testis in mice (Kwon et al., 2004). Thus, the functional diversity between UCH-L1 and UCH-L3 should also be defined. In addition to neurodegeneration, UCH-L1 is thought to be involved in the regulation of ATP receptors in neurons (Manago et al., 2005), in the morphology of neuronal precursors (Sakurai et al., 2006), in the normal function of the testis and the ovary (Kwon et al., 2005; Sekiguchi et al., 2006) and in various human diseases such as cancer (Hibi et al., 1999). Thus, UCH-L1 might contribute to more diverse phenomena than were previously thought.

Acknowledgements

The authors thank Dr. Tomohiro Kabuta and Dr. Satoshi Nagamine for their helpful comments. This work was supported in part by Grants-in-Aid for Scientific Research from the Ministry of Health, Labour and Welfare of Japan, Grants-in-Aid for Scientific Research from the Ministry of Education, Culture, Sports, Science and Technology of Japan, the Program for Promotion of Fundamental Studies in Health Sciences of the National Institute of Biomedical Innovation, and a grant from Japan Science and Technology Agency.

References

Ardley, H.C., Scott, G.B., Rose, S.A., Tan, N.G., Robinson, P.A., 2004. UCH-L1 aggresome formation in response to proteasome impairment indicates a role in inclusion formation in Parkinson's disease. J. Neurochem. 90, 379–391.

Butterfield, D.A., Gnjec, A., Poon, H.F., Castegna, A., Pierce, W.M., Klein, J.B., Martins, R.N., 2006. Redox proteomics identification of oxidatively modified brain proteins in inherited Alzheimer's disease: an initial assessment. J. Alzheimers Dis. 10, 391–397.

Caballero, O.L., Resto, V., Patturajan, M., Meerzaman, D., Guo, M.Z., Engles, J., Yochem, R., Ratovitski, E., Sidransky, D., Jen, J., 2002. Interaction and colocalization of PGP9.5 with JAB1 and p27(Kip1). Oncogene 21, 3003–3010.

Carmine Belin, A., Westerlund, M., Bergman, O., Nissbrandt, H., Lind, C., Sydow, O., Galter, D., 2007. S18Y in ubiquitin carboxy-terminal hydrolase L1 (UCH-L1) associated with decreased risk of Parkinson's disease in Sweden. Parkinsonism Relat. Disord. 13, 295–298.

Castegna, A., Aksenov, M., Thongboonkerd, V., Klein, J.B., Pierce, W.M., Booze, R., Markesbery, W.R., Butterfield, D.A., 2002. Proteomic identification of oxidatively modified proteins in Alzheimer's disease brain. Part II: Dihydropyrimidinase-related protein 2, alpha-enolase and heat shock cognate 71. J. Neurochem. 82, 1524–1532.

Castellani, R.J., Perry, G., Siedlak, S.L., Nunomura, A., Shimohama, S., Zhang, J., Montine, T., Sayre, L.M., Smith, M.A., 2002. Hydroxynonenal adducts indicate a role for lipid peroxidation in neocortical and brainstem Lewy bodies in humans. Neurosci. Lett. 319, 25–28.

Choi, J., Levey, A.I., Weintraub, S.T., Rees, H.D., Gearing, M., Chin, L.S., Li, L., 2004. Oxidative modifications and down-regulation of ubiquitin carboxyl-terminal hydrolase L1 associated with idiopathic Parkinson's and Alzheimer's diseases. J. Biol. Chem. 279, 13256–13264.

Cole, R.N., Hart, G.W., 2001. Cytosolic *O*-glycosylation is abundant in nerve terminals. J. Neurochem. 79, 1080–1089.

Das, C., Hoang, Q.Q., Kreinbring, C.A., Luchansky, S.J., Meray, R.K., Ray, S.S., Lansbury, P.T., Ringe, D., Petsko, G.A., 2006. Structural basis for conformational plasticity of the Parkinson's disease-associated ubiquitin hydrolase UCH-L1. Proc. Natl. Acad. Sci. U.S.A. 103, 4675–4680.

Elbaz, A., Levecque, C., Clavel, J., Vidal, J.S., Richard, F., Correze, J.R., Delemotte, B., Amouyel, P., Alperovitch, A., Chartier-Harlin, M.C., Tzourio, C., 2003. S18Y polymorphism in the UCH-L1 gene and Parkinson's disease: evidence for an age-dependent relationship. Mov. Disord. 18, 130–137.

Facheris, M., Strain, K.J., Lesnick, T.G., de Andrade, M., Bower, J.H., Ahlskog, J.E., Cunningham, J.M., Lincoln, S., Farrer, M.J., Rocca, W.A., Maraganore, D.M., 2005. UCHL1 is associated with Parkinson's disease: a case-unaffected sibling and case-unrelated control study. Neurosci. Lett. 381, 131–134.

Gong, B., Cao, Z., Zheng, P., Vitolo, O.V., Liu, S., Staniszewski, A., Moolman, D., Zhang, H., Shelanski, M., Arancio, O., 2006. Ubiquitin hydrolase Uch-L1 rescues beta-amyloid-induced decreases in synaptic function and contextual memory. Cell 126, 775–788.

Halliwell, B., 2006. Oxidative stress and neurodegeneration: where are we now? J. Neurochem. 97, 1634–1658.

Harada, T., Harada, C., Wang, Y.L., Osaka, H., Amanai, K., Tanaka, K., Takizawa, S., Setsuie, R., Sakurai, M., Sato, Y., Noda, M., Wada, K., 2004. Role of ubiquitin carboxy terminal hydrolase-L1 in neural cell apoptosis induced by ischemic retinal injury in vivo. Am. J. Pathol. 164, 59–64.

Healy, D.G., Abou-Sleiman, P.M., Casas, J.P., Ahmadi, K.R., Lynch, T., Gandhi, S., Muqit, M.M., Foltynie, T., Barker, R., Bhatia, K.P., Quinn, N.P., Lees, A.J., Gibson, J.M., Holton, J.L., Revesz, T., Goldstein, D.B., Wood, N.W., 2006. UCHL-1 is not a Parkinson's disease susceptibility gene. Ann. Neurol. 59, 627–633.

Hibi, K., Westra, W.H., Borges, M., Goodman, S., Sidransky, D., Jen, J., 1999. PGP9.5 as a candidate tumor marker for non-small-cell lung cancer. Am. J. Pathol. 155, 711–715.

Ichihara, N., Wu, J., Chui, D.H., Yamazaki, K., Wakabayashi, T., Kikuchi, T., 1995. Axonal degeneration promotes abnormal accumulation of amyloid beta-protein in ascending gracile tract of gracile axonal dystrophy (GAD) mouse. Brain Res. 695, 173–178.

Kwon, J., Mochida, K., Wang, Y.L., Sekiguchi, S., Sankai, T., Aoki, S., Ogura, A., Yoshikawa, Y., Wada, K., 2005. Ubiquitin C-terminal hydrolase L-1 is essential for the early apoptotic wave of germinal cells and for sperm quality control during spermatogenesis. Biol. Reprod. 73, 29–35.

Kwon, J., Wang, Y.L., Setsuie, R., Sekiguchi, S., Sato, Y., Sakurai, M., Noda, M., Aoki, S., Yoshikawa, Y., Wada, K., 2004. Two closely related ubiquitin C-terminal hydrolase isozymes function as reciprocal modulators of germ cell apoptosis in cryptorchid testis. Am. J. Pathol. 165, 1367–1374.

Larsen, C.N., Krantz, B.A., Wilkinson, K.D., 1998. Substrate specificity of deubiquitinating enzymes: ubiquitin C-terminal hydrolases. Biochemistry 37, 3358–3368.

Leroy, E., Boyer, R., Auburger, G., Leube, B., Ulm, G., Mezey, E., Harta, G., Brownstein, M.J., Jonnalagada, S., Chernova, T., Dehejia, A., Lavedan, C., Gasser, T., Steinbach, P.J., Wilkinson, K.D., Polymeropoulos, M.H., 1998. The ubiquitin pathway in Parkinson's disease. Nature 395, 451–452.

Levecque, C., Destee, A., Mouroux, V., Becquet, E., Defebvre, L., Amouyel, P., Chartier-Harlin, M.C., 2001. No genetic association of the ubiquitin carboxy-terminal hydrolase-L1 gene S18Y polymorphism with familial Parkinson's disease. J. Neural. Transm. 108, 979–984.

Lin, M.T., Beal, M.F., 2006. Mitochondrial dysfunction and oxidative stress in neurodegenerative diseases. Nature 443, 787–795.

Liu, Y., Fallon, L., Lashuel, H.A., Liu, Z., Lansbury Jr., P.T., 2002. The UCH-L1 gene encodes two opposing enzymatic activities that affect alpha-synuclein degradation and Parkinson's disease susceptibility. Cell 111, 209–218.

Lowe, J., McDermott, H., Landon, M., Mayer, R.J., Wilkinson, K.D., 1990. Ubiquitin carboxyl-terminal hydrolase (PGP9.5) is selectively present in ubiquitinated inclusion bodies characteristic of human neurodegenerative diseases. J. Pathol. 161, 153–160.

Manago, Y., Kanahori, Y., Shimada, A., Sato, A., Amano, T., Sato-Sano, Y., Setsuie, R., Sakurai, M., Aoki, S., Wang, Y.L., Osaka, H., Wada, K., Noda, M., 2005. Potentiation of ATP-induced currents due to the activation of P2X receptors by ubiquitin carboxy-terminal hydrolase L1. J. Neurochem. 92, 1061–1072.

Maraganore, D.M., Farrer, M.J., Hardy, J.A., Lincoln, S.J., McDonnell, S.K., Rocca, W.A., 1999. Case-control study of the ubiquitin carboxy-terminal hydrolase L1 gene in Parkinson's disease. Neurology 53, 1858–1860.

Maraganore, D.M., Lesnick, T.G., Elbaz, A., Chartier-Harlin, M.C., Gasser, T., Kruger, R., Hattori, N., Mellick, G.D., Quattrone, A., Satoh, J., Toda, T., Wang, J., Ioannidis, J.P., de Andrade, M., Rocca, W.A., 2004. UCHL1 is a Parkinson's disease susceptibility gene. Ann. Neurol. 55, 512–521.

Mellick, G.D., Silburn, P.A., 2000. The ubiquitin carboxy-terminal hydrolase-L1 gene S18Y polymorphism does not confer protection against idiopathic Parkinson's disease. Neurosci. Lett. 293, 127–130.

Meray, R.K., Lansbury Jr., P.T., 2007. Reversible monoubiquitination regulates the Parkinson's disease-associated ubiquitin hydrolase UCH-L1. J. Biol. Chem. 282, 10567–10575.

Montine, K.S., Olson, S.J., Amarnath, V., Whetsell Jr., W.O., Graham, D.G., Montine, T.J., 1997. Immunohistochemical detection of 4-hydroxy-2-nonenal adducts in Alzheimer's disease is associated with inheritance of APOE4. Am. J. Pathol. 150, 437–443.

Naito, S., Mochizuki, H., Yasuda, T., Mizuno, Y., Furusaka, M., Ikeda, S., Adachi, T., Shimizu, H.M., Suzuki, J., Fujiwara, S., Okada, T., Nishikawa, K., Aoki, S., Wada, K., 2006. Characterization of multimetric variants of ubiquitin carboxyl-terminal hydrolase L1 in water by small-angle neutron scattering. Biochem. Biophys. Res. Commun. 339, 717–725.

Nijman, S.M., Luna-Vargas, M.P., Velds, A., Brummelkamp, T.R., Dirac, A.M., Sixma, T.K., Bernards, R., 2005. A genomic and functional inventory of deubiquitinating enzymes. Cell 123, 773–786.

Nishikawa, K., Li, H., Kawamura, R., Osaka, H., Wang, Y.L., Hara, Y., Hirokawa, T., Manago, Y., Amano, T., Noda, M., Aoki, S., Wada, K., 2003. Alterations of structure and hydrolase activity of parkinsonism-associated human ubiquitin carboxyl-terminal hydrolase L1 variants. Biochem. Biophys. Res. Commun. 304, 176–183.

Osaka, H., Wang, Y.L., Takada, K., Takizawa, S., Setsuie, R., Li, H., Sato, Y., Nishikawa, K., Sun, Y.J., Sakurai, M., Harada, T., Hara, Y., Kimura, I., Chiba, S., Namikawa, K., Kiyama, H., Noda, M., Aoki, S., Wada, K., 2003. Ubiquitin carboxy-terminal hydrolase L1 binds to and stabilizes monoubiquitin in neuron. Hum. Mol. Genet. 12, 1945–1958.

Saigoh, K., Wang, Y.L., Suh, J.G., Yamanishi, T., Sakai, Y., Kiyosawa, H., Harada, T., Ichihara, N., Wakana, S., Kikuchi, T., Wada, K., 1999. Intragenic deletion in the gene encoding ubiquitin carboxy-terminal hydrolase in gad mice. Nat. Genet. 23, 47–51.

Sakurai, M., Ayukawa, K., Setsuie, R., Nishikawa, K., Hara, Y., Ohashi, H., Nishimoto, M., Abe, T., Kudo, Y., Sekiguchi, M., Sato, Y., Aoki, S., Noda, M., Wada, K., 2006. Ubiquitin C-terminal hydrolase L1 regulates the morphology of neural progenitor cells and modulates their differentiation. J. Cell Sci. 119, 162–171.

Sano, Y., Furuta, A., Setsuie, R., Kikuchi, H., Wang, Y.L., Sakurai, M., Kwon, J., Noda, M., Wada, K., 2006. Photoreceptor cell apoptosis in the retinal degeneration of Uchl3-deficient mice. Am. J. Pathol. 169, 132–141.

Sekiguchi, S., Kwon, J., Yoshida, E., Hamasaki, H., Ichinose, S., Hideshima, M., Kuraoka, M., Takahashi, A., Ishii, Y., Kyuwa, S., Wada, K., Yoshikawa, Y., 2006. Localization of ubiquitin C-terminal hydrolase L1 in mouse ova and its function in the plasma membrane to block polyspermy. Am. J. Pathol. 169, 1722–1729.

Semenova, E., Wang, X., Jablonski, M.M., Levorse, J., Tilghman, S.M., 2003. An engineered 800 kilobase deletion of Uchl3 and Lmo7 on mouse

chromosome 14 causes defects in viability, postnatal growth and degeneration of muscle and retina. Hum. Mol. Genet. 12, 1301–1312.

Setsuie, R., Wang, Y.L., Mochizuki, H., Osaka, H., Hayakawa, H., Ichihara, N., Li, H., Furuta, A., Sano, Y., Sun, Y.J., Kwon, J., Kabuta, T., Yoshimi, K., Aoki, S., Mizuno, Y., Noda, M., Wada, K., 2007. Dopaminergic neuronal loss in transgenic mice expressing the Parkinson's disease-associated UCH-L1 I93M mutant. Neurochem. Int. 50, 119–129.

Tan, E.K., Puong, K.Y., Fook-Chong, S., Chua, E., Shen, H., Yuen, Y., Pavanni, R., Wong, M.C., Puvan, K., Zhao, Y., 2006. Case-control study of UCHL1 S18Y variant in Parkinson's disease. Mov. Disord. 21, 1765–1768.

Toda, T., Momose, Y., Murata, M., Tamiya, G., Yamamoto, M., Hattori, N., Inoko, H., 2003. Toward identification of susceptibility genes for sporadic Parkinson's disease. J. Neurol. 250 (Suppl. 3), III40–III43.

Wang, J., Zhao, C.Y., Si, Y.M., Liu, Z.L., Chen, B., Yu, L., 2002. ACT and UCH-L1 polymorphisms in Parkinson's disease and age of onset. Mov. Disord. 17, 767–771.

Wilkinson, K.D., Lee, K.M., Deshpande, S., Duerksen-Hughes, P., Boss, J.M., Pohl, J., 1989. The neuron-specific protein PGP9.5 is a ubiquitin carboxyl-terminal hydrolase. Science 246, 670–673.

Wilson, P.O., Barber, P.C., Hamid, Q.A., Power, B.F., Dhillon, A.P., Rode, J., Day, I.N., Thompson, R.J., Polak, J.M., 1988. The immunolocalization of protein gene product 9.5 using rabbit polyclonal and mouse monoclonal antibodies. Br. J. Exp. Pathol. 69, 91–104.

Wintermeyer, P., Kruger, R., Kuhn, W., Muller, T., Woitalla, D., Berg, D., Becker, G., Leroy, E., Polymeropoulos, M., Berger, K., Przuntek, H., Schols, L., Epplen, J.T., Riess, O., 2000. Mutation analysis and association studies of the UCHL1 gene in German Parkinson's disease patients. Neuroreport 11, 2079–2082.

Yoritaka, A., Hattori, N., Uchida, K., Tanaka, M., Stadtman, E.R., Mizuno, Y., 1996. Immunohistochemical detection of 4-hydroxynonenal protein adducts in Parkinson disease. Proc. Natl. Acad. Sci. U.S.A. 93, 2696–2701.

Available online at www.sciencedirect.com
ScienceDirect
Bioorganic & Medicinal Chemistry
ELSEVIER
Bioorganic & Medicinal Chemistry 15 (2007) 6810–6818

Identification of novel chemical inhibitors for ubiquitin C-terminal hydrolase-L3 by virtual screening

Kazunori Hirayama,[a,b] Shunsuke Aoki,[b,*] Kaori Nishikawa,[b] Takashi Matsumoto[a] and Keiji Wada[b]

[a]*Department of Electrical Engineering and Bioscience, Graduate School of Advanced Science and Engineering, Waseda University, 3-4-1 Okubo, Shinjuku-ku, Tokyo 169-8555, Japan*
[b]*Department of Degenerative Neurological Diseases, National Institute of Neuroscience, National Center of Neurology and Psychiatry, 4-1-1 Ogawa-Higashi, Kodaira, Tokyo 187-8502, Japan*

Received 11 May 2007; revised 14 July 2007; accepted 18 July 2007
Available online 19 August 2007

Abstract—UCH-L3 (ubiquitin C-terminal hydrolase-L3) is a de-ubiquitinating enzyme that is a component of the ubiquitin–proteasome system and known to be involved in programmed cell death. A previous study of high-throughput drug screening identified an isatin derivative as a UCH-L3 inhibitor. In this study, we attempted to identify a novel inhibitor with a different structural basis. We performed in silico structure-based drug design (SBDD) using human UCH-L3 crystal structure data (PDB code; 1XD3) and the virtual compound library (ChemBridge CNS-Set), which includes 32,799 chemicals. By a two-step virtual screening method using DOCK software (first screening) and GOLD software (second screening), we identified 10 compounds with GOLD scores of over 60. To address whether these compounds exhibit an inhibitory effect on the de-ubiquitinating activity of UCH-L3, we performed an enzymatic assay using ubiquitin-7-amido-4-methylcoumarin (Ub-AMC) as the substrate. As a result, we identified three compounds with similar basic dihydro-pyrrole skeletons as UCH-L3 inhibitors. These novel compounds may be useful for the research of UCH-L3 function, and in drug development for UCH-L3-associated diseases.

1. Introduction

The ubiquitin–proteasome system is responsible for the regulation of cellular proteolysis. In this system, ubiquitination serves as a targeting signal for proteolysis.[1] Ubiquitin C-terminal hydrolase-L3 (UCH-L3) is one of the components of the ubiquitin–proteasome system and hydrolyzes ubiquitin C-terminal adducts for the recycling of cellular ubiquitin.[2] Ubiquitin with C-terminal adducts is a substrate for UCH-L3, and ubiquitin with a free C-terminus is recycled within the ubiquitin–proteasome system. There is some evidence that UCH-L3 plays an important role in programmed cell death. Programmed cell death is implicated in a number of human diseases, including neurodegenerative disease,[3] autoimmune disease,[4] cancers[5,6], etc. Loss of UCH-L3 leads to programmed cell death by apoptosis of certain type of cells in vivo, germ line cells and photoreceptor cells.[7,8] High-level expression of UCH-L3 genes and proteins, and acceleration of UCH-L3 enzymatic activity is reported in multiple types of cancer cells,[5,6] suggesting that UCH-L3 activity may be required for cancer cell survival. Therefore, UCH-L3 is a potential target for drug development to control programmed cell death in specific types of cells including cancer cells.

Structure-based drug design (SBDD) is a method used to discover novel leads for drug development as it enables more rapid hit identification than the classical screening methods of in vitro or in vivo biological assays. The computer-based approach for drug screening, using molecular docking, is a shortcut method when the crystal structure of a target protein is available. Key methodologies for docking small molecules to protein were developed during the early 1980s,[9] and various types of docking simulation software are now available, for example, DOCK,[10] GOLD, and FlexX.[11] BCR-ABL tyrosine kinase inhibitors (IC_{50} values ranging from 10 to 200 μM) were successfully

Keywords: UCH-L3; Dihydro-pyrrole; Structure-based drug design; Virtual screening.
* Corresponding author. Tel.: +81 42 341 2712x5144; fax: +81 42 346 1745; e-mail: aokis@ncnp.go.jp

0968-0896/$ - see front matter © 2007 Elsevier Ltd. All rights reserved.
doi:10.1016/j.bmc.2007.07.016

identified by virtual screening of 200,000 compounds against crystal structures using DOCK,[12] implemented by the anchor-and-grow algorithm with respect to ligand flexibility.[10] Human thymidine phosphorylase inhibitor (IC_{50} = 77 μM) was also identified by virtual screening of 250,521 compounds using DOCK.[13] Furthermore, metallo-β-lactamase inhibitors (IC_{50} values less than 15 μM) were identified through virtual screening by GOLD,[14] using the genetic algorithm for ligand flexibility.

The advantage of chaining different docking programs was evaluated and the results suggested that virtual ligand screening is performed faster with reasonable accuracy by using chained screening, than by using a single program with default parameters.[15] In this study, the results of chained docking against UCH-L3 crystal structure were examined by UCH-L3 hydrolysis activity assay to validate the efficacy of the DOCK–GOLD SBDD method. We identified three inhibitors (IC_{50} = 100–150 μM) of UCH-L3 by the DOCK–GOLD virtual screening of 32,799 compounds.

2. Results and discussion

2.1. Protein preparation and chemical database

In the 3D structure of the UCH-L3-ubiquitin complex, ubiquitin C-terminus is buried in the active site cleft among four active site residues of UCH-L3: Gln89, Cys95, His169, and Asp184.[16,17] During the virtual screening process by DOCK and GOLD, the protein–ligand interacting site was restricted to the binding site of the three ubiquitin C-terminal amino residues (as described in Section 4), in order that the outcome could be verified by a ubiquitin C-terminal hydrolase enzymatic assay. The first DOCK screening was performed against 32,799 compounds of CNS-Set, which was prefiltered by RPBS under the most modest filtering condition.[18]

2.2. DOCK and GOLD screenings

To screen for compounds that bind to the active site, the first screening was performed by DOCK, and the protein–ligand interaction area was restricted to the ubiquitin binding site of UCH-L3 (see Section 4). The top-scoring 1780 compounds (5.4% of the initial 32,799 compounds) with energy scores of less than −30 kcal/mol were selected for further screening. These compounds were then re-screened by GOLD twice, with different genetic algorithm (GA) settings. To predict binding ability to the active site cleft accurately, the protein–ligand interacting area was defined in approximately the same way as in the first DOCK screening step (see Section 4). Screening by GOLD consisted of two rounds. Using the GOLD score, we initially extracted the top scoring 100 compounds from 1780 compounds, using the 7–8 times speed-up GA parameter settings. These 100 compounds were then re-scored using the default GA settings (see Section 4) to more accurately predict binding ability. Ten compounds with GOLD scores of over 60 were predicted to bind to the UCH-L3 active site; that is, 0.03% of the total number of chemical compounds was screened.

2.3. IC_{50} determination

A previous study demonstrated that compounds with GOLD scores of about 60 may inhibit enzyme activity with IC_{50} values of 10–100 μM.[19] An enzyme assay was performed among the top 10 chemicals to address whether they actually bind to the UCH-L3 active site with the predicted affinities (Table 1 and Fig. 1).

Ubiquitin-7-amido-4-methylcoumarin (Ub-AMC; AMC attaches to the carboxyl terminus of ubiquitin) is a fluorogenic substrate of UCH-L3 and other UCH isozymes. UCH-L3 is known to hydrolyze Ub-AMC into free ubiquitin and AMC,[20,21] and the hydrolyzed AMC group is excited at light wavelength of 355 nm and emits fluorescence at 460 nm. Hydrolysis activity of UCH-L3 is inhibited if a compound binds to its active site and thus blocks interaction between the active site of UCH-L3 and the ubiquitin C-terminus. Inhibition of hydrolysis of Ub-AMC leads to a lower concentration of free AMC and hence a lower level of fluorescence intensity.

We experimentally determined the affinity constant (K_m) of Ub-AMC hydrolysis by human UCH-L3 as 83.3 ± 1.5 nM (mean ± SEM, from three independent experiments). The candidate compounds identified by

Table 1. GOLD scores of the top 10 ranked chemicals after GOLD calculation[a]

Docking rank/Compound No.	Compound name	GOLD scores
1	1-Benzyl-3-hydroxy-4-(5-methyl-2-furoyl)-5-(3-pyridinyl)-1,5-dihydro-2*H*-pyrrol-2-one	66.01
2	3-[4-Methyl-5-({[3-(2-thienyl)-1,2,4-oxadiazol-5-yl]methyl}thio)-4*H*-1,2,4-triazol-3-yl]-1*H*-indole	65.62
3	*N*-{4-[1-(2-Furoyl)-5-(2-furyl)-4,5-dihydro-1*H*-pyrazol-3-yl]phenyl}methanesulfonamide	64.85
4	N^1-Cyclopropyl-N^2-(4-methoxyphenyl)-N^2-[(4-methylphenyl)sulfonyl]glycinamide	64.76
5	*N*-{3-[1-Acetyl-5-(2-thienyl)-4,5-dihydro-1*H*-pyrazol-3-yl]phenyl}ethanesulfonamide	64.23
6	3-Hydroxy-5-(4-methoxyphenyl)-1-(1,3,4-thiadiazol-2-yl)-4-(2-thienylcarbonyl)-1,5-dihydro-2*H*-pyrrol-2-one	62.96
7	5-(4-Fluorophenyl)-3-hydroxy-4-(5-methyl-2-furoyl)-1-(3-pyridinylmethyl)-1,5-dihydro-2*H*-pyrrol-2-one	62.73
8	N^1-Cyclopropyl-N^2-[(4-methoxyphenyl)sulfonyl]-N^2-(4-methylphenyl)glycinamide	62.52
9	N^1-Cyclopentyl-N^2-(3-methoxyphenyl)-N^2-(phenylsulfonyl)glycinamide	62.39
10	4-({[5-(2-Furyl)-4-phenyl-4*H*-1,2,4-triazol-3-yl]thio}methyl)-1,3-thiazol-2-amine	62.35

[a] Ten compounds are listed according to the top 10 rank of GOLD scores and assigned the number corresponding to GOLD score ranks.

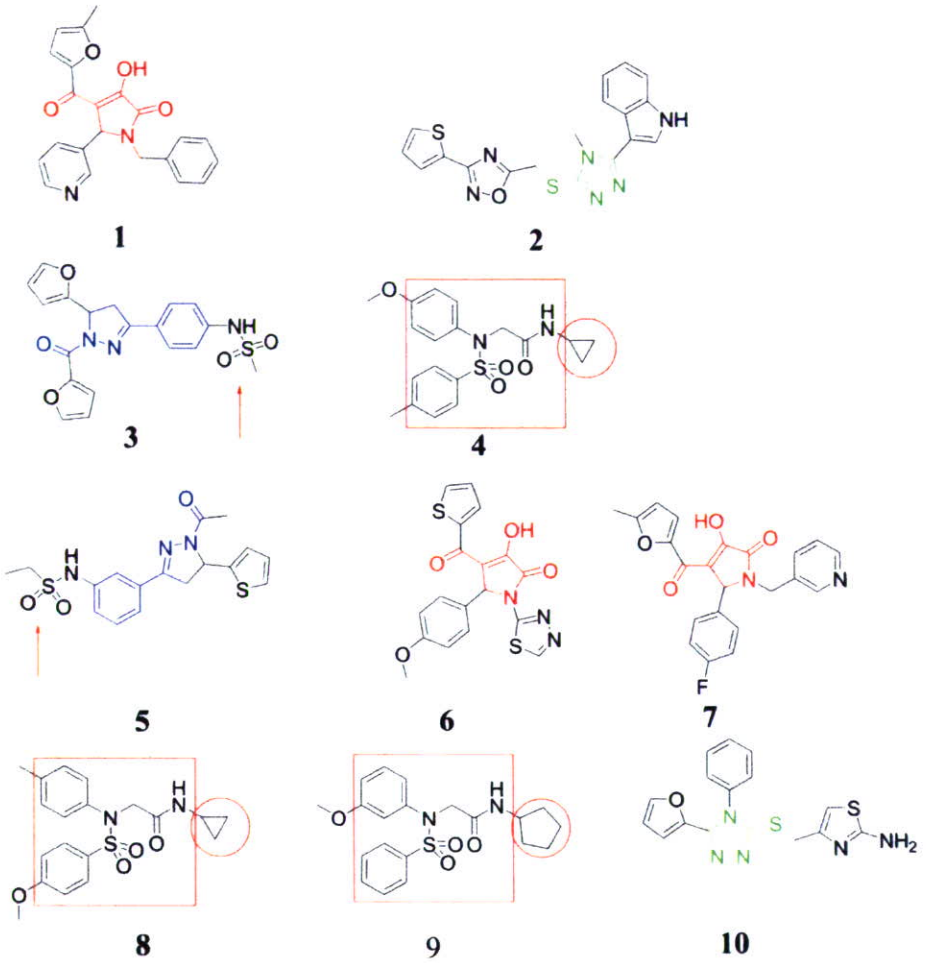

Figure 1. Top 10 ranked compounds identified by DOCK and GOLD screening. Note that there are several shared basic skeletons and functional groups: 1,5-dihydro-2*H*-pyrrol-2-one (drawn in red, compounds **1**, **6**, and **7**), glycinamide (boxed in red, compounds **4**, **8**, and **9**), cycloalkane group (circled in red, compounds **4** and **8**; cyclopropyl, compound **9**; cyclopentyl), 4,5-dihydro-1*H*-pyrazol-3-yl phenyl (drawn in blue, compounds **3** and **5**), sulfonamide (pointed, compounds **3** and **5**), and 4*H*-1,2,4-triazol-3-yl (drawn in green, compounds **2** and **10**).

DOCK–GOLD chained docking screening were tested for their ability to inhibit the hydrolysis activity of UCH-L3, at the Ub-AMC concentration equivalent to the K_m value. Four compounds among these candidates inhibited enzyme activity (Fig. 2a). We did not test the inhibitory effects of compound **3**, as it is a fluorogenic chemical with an emission wavelength of 460 nm. Compounds **1**, **6**, and **7** significantly inhibited the hydrolysis activity of UCH-L3 (initial velocity of Ub-AMC hydrolysis; nM/s [Fig. 2b]). Compounds **1** (401 μM), **6** (375 μM), and **7** (350 μM) inhibited the hydrolysis activity by 83.2 ± 1.5%, 76.5 ± 0.6%, and 76.8 ± 1.0%, respectively, as compared with control DMSO ($p < 0.01$, vs control; Dunnett's test). The IC_{50} value of compound **2** should hypothetically be several hundred μM. Although compound **2** (380 μM) inhibited hydrolysis activity by 16.2 ± 2.1% as compared with control DMSO, the difference was not found to be significant by Dunnett's test. Five other compounds were unable to inhibit the UCH-L3 hydrolysis activity: compound **4** (334 μM; final concentration), compound **5** (331 μM), compound **8** (401 μM), compound **9** (386 μM), and compound **10** (387 μM) (Fig. 2b). Experimentally determined IC_{50} values of compounds **1**, **6**, and **7** (Fig. 3) were as follows: compound **1** (103 μM), compound **6** (154 μM), and compound **7** (123 μM).

2.4. Competitive inhibitor

To show that the identified compounds bind to the active site of the UCH-L3, various concentrations of compound **1** and iodoacetamide (108 mM) were added to UCH-L3/Ub-AMC reaction buffer. Iodoacetamide is a non-competitive inhibitor of UCH-L3 (Fig. 4a). It is a thiol alkylating agent of the UCH-L family and derivatizes and inactivates the active site leading to loss of UCH-L3 enzymatic activity.[22] In the presence of compound **1** and iodoacetamide, the percentage of active UCH-L3 reduced by iodoacetamide treatment was recovered in comparison with the control, and the recovery was dependent on the concentration of compound **1** (Fig. 4b). Our results showed that compound **1** is a competitive inhibitor of UCH-L3. This suggests that compound **1** bound to the UCH-L3 active site to prevent iodoacetamide from inactivating it.

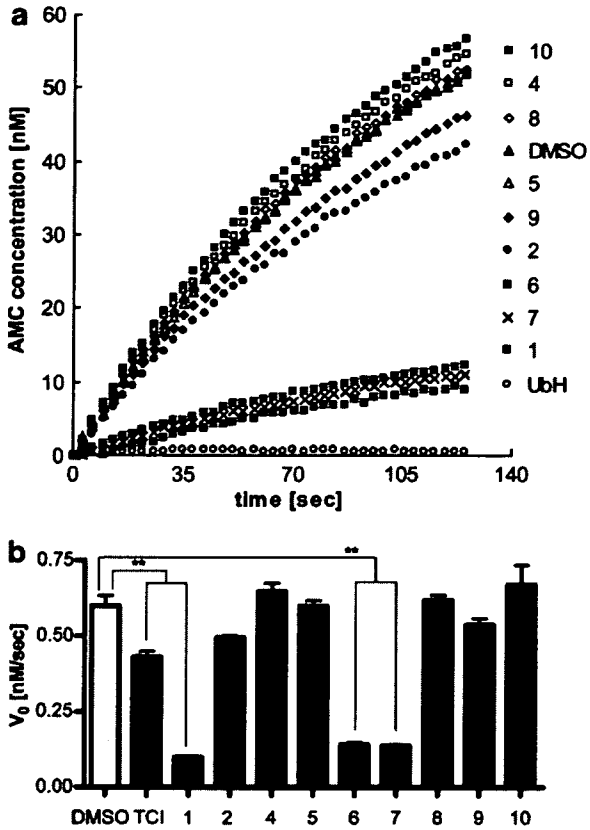

Figure 2. Analysis of UCH-L3 inhibitory effects of compounds 1–10. (a) Kinetics of UCH-L3-catalyzed hydrolysis of Ub-AMC with the compounds. Fluorescence intensity was converted to AMC concentration by subtracting the intensity of fully hydrolyzed substrate from that of solution without substrate. Concentrations of compounds are as follows: compound **1** (401 μM); compound **2** (380 μM); compound **4** (334 μM); compound **5** (331 μM); compound **6** (375 μM); compound **7** (350 μM); compound **8** (401 μM); compound **9** (386 μM); and compound **10** (387 μM). As a known inhibitor, ubiquitin-aldehyde (Ub-H, 120 nM) was used. Each value represents the mean of three independent experiments. (b) Inhibitory effects of compounds on initial velocity of hydrolysis (V_0) are shown. Fluorescence intensity was converted by the same method described in (a). 4,5,6,7-Tetrachloroindan-1,3-dione (TCI, 20 μM) was used as a UCH-L3 selective inhibitor with IC_{50} of 600 nM.[22] Each value represents the mean ± SEM of three independent experiments. Dunnett's multiple comparison test was performed using GraphPad Prism software (**: $p < 0.01$, DMSO as control).[29]

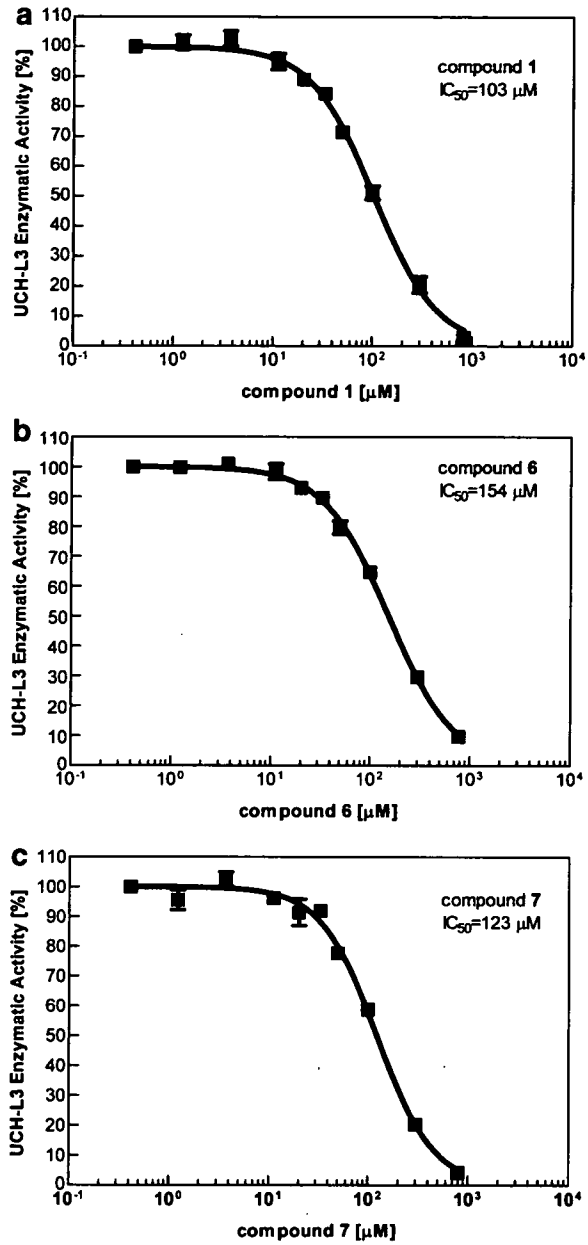

Figure 3. IC_{50} curves of compounds for UCH-L3 enzymatic activity. (a) Compound **1**, (b) compound **6**, and (c) compound **7**. The horizontal axis shows the concentration of each compound. The vertical axis shows the relative UCH-L3 enzymatic activity [%] in comparison with maximal initial velocity. IC_{50} values are shown in graphs. Each plotted value represents the mean ± SEM of three independent experiments.

In order to show that the compounds **1**, **6**, and **7** bind to UCH-L3, Biacore 100 analysis was conducted. Biacore 100 analysis detects interaction between a small molecule and protein and enables quantification of the interaction.[23] The results showed that binding of each compound to UCH-L3 increased and was dependent on the concentration of the compound **6** (data not shown).

2.5. Predicted binding mode

Figure 5 shows the predicted binding modes of compounds **1**, **6**, and **7** to UCH-L3. Since chemical formulae of the three compounds are similar to each other, the predicted docked structures of these and UCH-L3 have similar binding modes. Two hydrogen bonds were observed between the docked ligand and two amino acid residues in the predicted compound **1**/UCH-L3 complex structure; the carbonyl group of compound **1** appears to form a hydrogen bond to the NH group of Ala11, and the pyrrole C=O appears to form a hydrogen bond to the hydroxyl group of Thr157. Three hydrogen bonds were predicted between the docked ligand and two amino acid residues in the compound **6**/UCH-L3 complex structure; the thiadiazole group of compound **6** appears to form a hydrogen bond to the NH group of Leu9, and

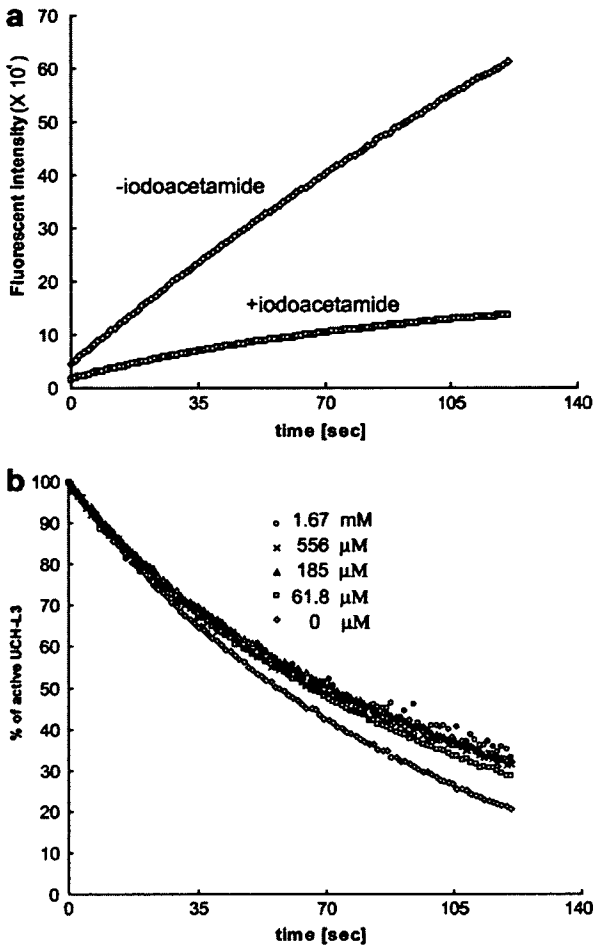

Figure 4. Competitive inhibition of compound **1**. (a) Kinetics of UCH-L3-catalyzed hydrolysis of Ub-AMC with or without iodoacetamide (108 mM). (b) Reaction progress curves normalized by final fluorescence intensity representing the ratio of active UCH-L3 (for calculations, see Section 4.9), in the presence of iodoacetamide (108 mM) and compound **1** (0 μM, 61.8 μM, 185 μM, 556 μM, and 1.67 mM).

the pyrrole hydroxyl group and pyrrole C=O appear to form a hydrogen bond to the NH group of Ala11. A hydrogen bond was observed between the docked ligand and the amino acid residues of UCH-L3 in the predicted compound **7**/UCH-L3 complex structure; the carbonyl group of compound **7** appears to form a hydrogen bond to the NH group of Ala11. The predicted binding mode of compound **10**, as a non-binder, was analyzed. Four hydrogen bonds were observed between the docked ligand and the amino acid residues of UCH-L3 in the predicted compound **10**/UCH-L3 complex structure. The triazol group of compound **10** appears to form two hydrogen bonds to the hydroxyl group of Thr157, and the amino group of compound **10** appears to form a hydrogen bond to the CO group of Glu154, and to the CO group of Ser151. Although hydrogen bonds between actual inhibitors (compounds **1**, **6**, and **7**) and Ala11 were observed, compound **10**, a non-inhibitor, does not appear to form a hydrogen bond to Ala11. This hydrogen bond might be important for compounds to bind stably to the UCH-L3 active site.

2.6. Discussion; analysis of active compounds

By three-step virtual screening (DOCK, high-speed GOLD, and low-speed GOLD) of 32,799 chemicals, we identified 10 candidate chemicals that potentially inhibit UCH-L3 hydrolysis activity. We examined the actual inhibitory effects of the compounds on UCH-L3 hydrolysis activity by biochemical enzymatic assay and identified three compounds (compounds **1**, **6**, and **7**) as UCH-L3 inhibitors, with IC_{50} values of 100–150 μM. By comparing the structural formulae of the three compounds, we found that the 1,5-dihydro-2*H*-pyrrol-2-one group is likely to be important for inhibition of UCH-L3-hydrolysis activity (Fig. 6). Several common structural features can be drawn from these three chemicals (Fig. 6). First, the heteroaromatic pyrrole group is common to all three compounds. Second, each of the three compounds also contains pyridines and furoyls as heteroaromatic functional groups. Third, a carbon–oxygen double bond at position 2, a hydroxyl group at position 3, a carbonyl group at position 4, and a hydrogen atom at position 5 of the pyrrole ring are common to each compound. Fourth, a five- or six-membered cyclic group at positions 1, 4, and 5 is common to all three chemicals (Fig. 6). Furthermore, compounds **1** and **7** have two heteroaromatic groups: a pyridinyl group and a furoyl group.

The structural similarities of UCH-L3-binding chemicals have an influence on binding mode similarities. There are two main pockets in the substrate-binding site of UCH-L3: the first pocket (Pocket 1) is formed by Pro8, Glu10, and Thr157 and the second pocket (Pocket 2), the active site pocket, is formed by Asp167, Leu168, and Cys90. Docked orientations of compounds **1** and **7** are very similar, as positions 1 and 5 six-membered cyclic groups fit into each pocket. This suggests that two features among these similarities are likely to be important for stable binding to the active site: a pyrrole ring and two heteroaromatic groups, which fit into both pockets around the UCH-L3 substrate-binding site. The shape of Pocket 1 is different from that of UCH-L1,[24] another isoform of the UCH family (52% amino acid sequence identity).[25] Thus, modification of the chemical groups in Pocket 1 might be effective during drug design, to enhance specificity for UCH-L3 over UCH-L1.

Several lines of evidence indicate that UCH-L3 is associated with tumorigenesis and carcinogenesis. High-level expression and activity of UCH-L3 has been reported in multiple types of cancer cells. Expression of UCH-L3 mRNA is upregulated in breast tumors and UCH-L3 mRNA levels are associated with the histological grading of such tumors.[5] Moreover, it has been suggested that the activity of UCH-L3 is also upregulated in the majority of cervical carcinoma tissues, compared with adjacent normal tissues.[6] On the other hand, loss of UCH-L3 is known to induce cell death in knock-out studies. UCH-L3 is involved in the protection of programmed cell death in germ cells and photoreceptor cells in vivo.[7,8] Thus, the structural information of the

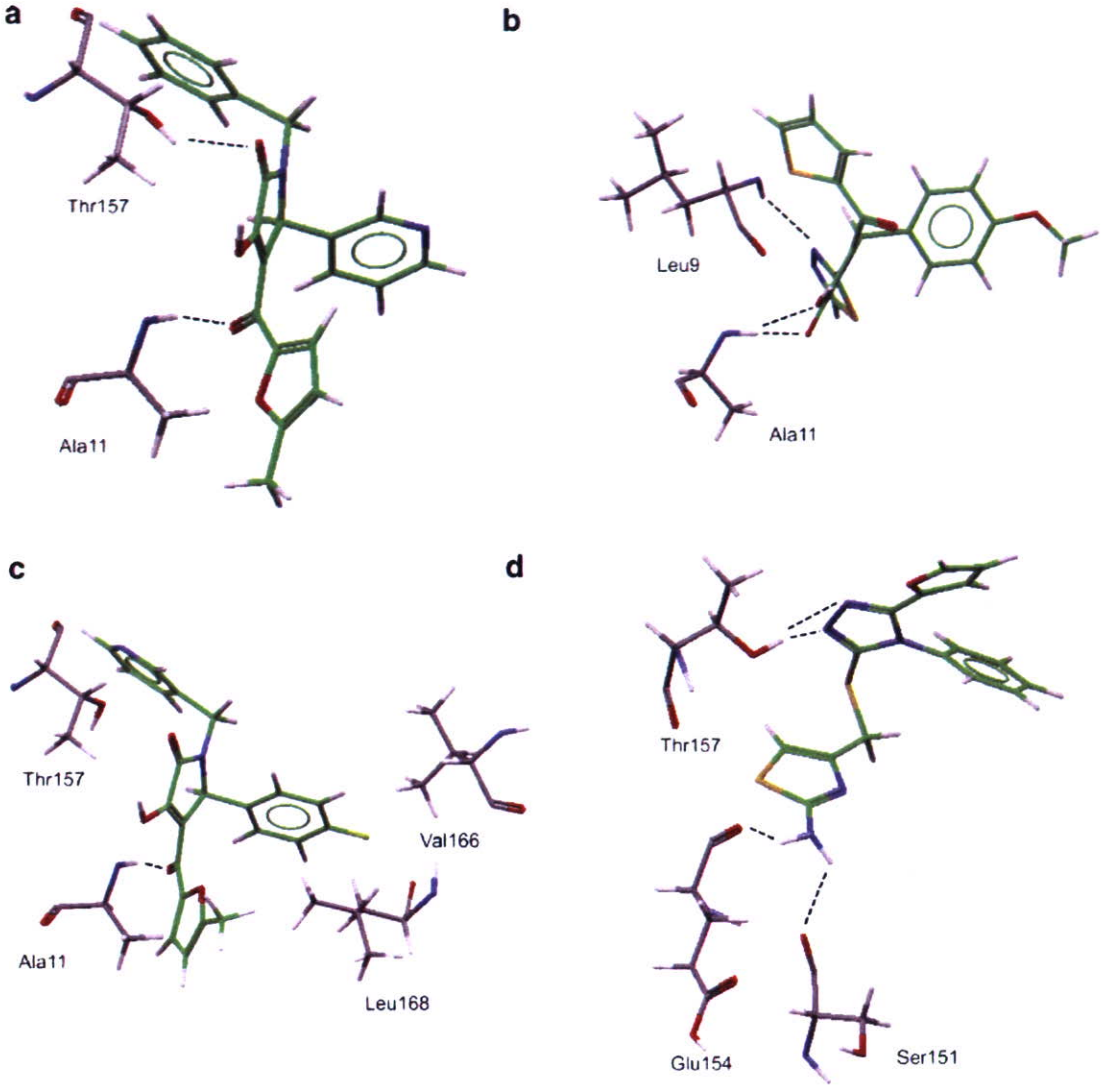

Figure 5. Illustration showing the molecular docking results. Docked orientation of (a) compound **1**, (b) compound **6**, (c) compound **7**, and (d) compound **10** in the UCH-L3 active site using GOLD and shown with interacting residues. Hydrogen bonds are shown by a dashed line. Oxygen atoms are shown in red, nitrogen atoms in blue, sulfur atoms in orange, fluorine atoms in yellow, and hydrogen atoms in gray. The enzyme carbons are shown in dark gray and those of the ligands in green.

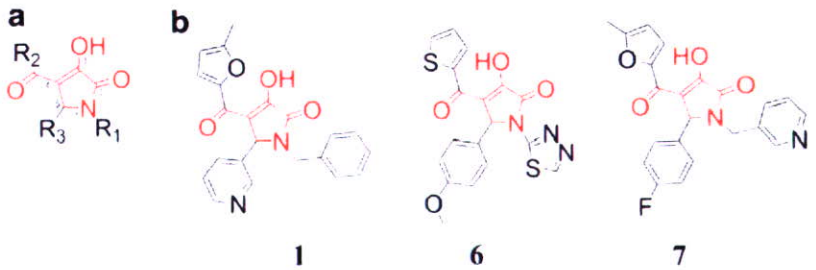

Figure 6. Structural similarities of the three compounds. (a) 1,5-Dihydro-2*H*-pyrrol-2-one group, the common basic skeleton, is shown in red. Position numbers of the pyrrole ring are shown as small characters. R_1–R_3 represent each functional group at positions 1, 4, and 5 of the pyrrole ring, respectively. (b) Structures of identified inhibitors: compounds **1**, **6**, and **7**.

UCH-L3 inhibitors we identified may be useful for future apoptosis-inducing anti-cancer drug development. UCH-L3 should be an important target for modulating cell apoptosis.

3. Conclusion

In this study, we employed three-step docking (DOCK, rough GOLD, and fine GOLD) and in vitro enzyme

assay methods, and identified three UCH-L3 inhibitors with IC_{50} values of 100–150 μM. These novel inhibitors have a dihydro-pyrrole group in common.

4. Experimental

4.1. Compound library

We used the ADME/Tox (absorption, distribution, metabolism, excretion, and toxicity) filtered virtual compound library (ChemBridge CNS-Set) which includes a collection of 32,799 chemical compounds.[18] All compounds satisfy Lipinski's Rule of five.

4.2. Protein preparation

Human UCH-L3 and ubiquitin vinylmethylester (Ub-VME) complex crystal structure data (PDB code; 1XD3) were obtained from Protein Data Bank (PDB).[17] Hydrogens were added to UCH-L3-ubiquitin complex using CVFF99 force field by Biopolymer module in Insight II 2000 suite (Accelrys, Inc., San Diego, CA). Energy was minimized by the Discover 3 module of the same suite with all heavy atoms restrained, except hydrogen, to relieve any short contacts. To use the UCH-L3 protein structure in the following docking simulations, the structures of UCH-L3 and Ub-VME complex were divided into their components.

4.3. Virtual screening

Virtual screening experiments were performed by UCSF DOCK 5.4.0[10] and GOLD 3.0.1 (CCDC, Cambridge, UK).[26] In the first screening by DOCK, the substrate-binding site was defined, by selecting ligand atom accessible spheres and describing molecular surfaces with the SPHERE_GENERATOR program in the DOCK suite. All spheres within 6 Å of root mean square deviation (RMSD) from every atom of the three C-terminal residues of energy-minimized ubiquitin were selected by the SPHERE_SELECTOR program in DOCK suite. A scoring function ($E_{int} = E_{vdw} + E_{elec}$) was used to estimate potential binding affinity. Following the first screening with rigid ligand conditions, 1780 compounds with binding energy scores of less than −30 kcal/mol were selected for a second screening by GOLD.

Using GOLD, the 1780 compounds were screened with 7–8 times speed-up settings; that is, the pre-defined genetic algorithm (GA) parameter settings to achieve calculation speed-up. The top-ranked 100 compounds were determined, then screened by default settings; the GA parameter settings for a slower calculation with greater ligand flexibility, but with a more accurate prediction. Ligand flexibility was turned on in both the 7–8 times speed-up settings and the default settings. Protein side chain flexibility was not turned on in any settings. The virtual tripeptide structure composed of three C-terminal residues of the energy-minimized ubiquitin was set as the reference ligand to define the ligand-binding site. All protein atoms within 5 Å of each ligand atom were used for defining the binding site. The solvent-accessible surfaces of the docking region were restricted by a cavity detection algorithm.[27] As a result, the binding site was composed of 174 active atoms (automatically selected by GOLD software). A method for defining the binding site with tripeptide yielded the best score among other methods using shorter or longer C-terminal peptide sequences of ubiquitin (data not shown). Ten docking solutions for each docked molecule were scored and the top three were saved for post-screening evaluations. Potential hydrogen bonds and van der Waals contacts were identified using Silver 1.0 (CCDC, Cambridge, UK).[28] Ligands predicted to be tight-binders by both DOCK and GOLD were applied to further in vitro experimental validation. All calculations were performed on seven Linux or Cygwin 2–3 GHz/Pentium IV CPU personal computers.

4.4. Statistical analysis

All statistical analysis was performed by GraphPad Prism 4 (GraphPad Software, Inc., San Diego, CA).[29]

4.5. Reagents

Human recombinant UCH-L3, ubiquitin-7-amido-4-methylcoumarin (Ub-AMC), and ubiquitin-aldehyde (Ub-H) were purchased from Boston Biochem, Inc. (Cambridge, MA). 4,5,6,7-Tetrachloroindan-1,3-dione (TCI) was purchased from Fisher Scientific International Inc. (Hampton, NH). Iodoacetamide was purchased from Sigma–Aldrich Corporation (St. Louis, MO). Compounds within ChemBridge CNS-Set (Supplier IDs given in parentheses) are as follows: compound **1**: 1-benzyl-3-hydroxy-4-(5-methyl-2-furoyl)-5-(3-pyridinyl)-1,5-dihydro-2*H*-pyrrol-2-one (7504601); compound **2**: 3-[4-methyl-5-({[3-(2-thienyl)-1,2,4-oxadiazol-5-yl]methyl}thio)-4*H*-1, 2,4-triazol-3-yl]-1*H*-indole (7950509); compound **3**: *N*-{4-[1-(2-furoyl)-5-(2-furyl)-4,5-dihydro-1*H*-pyrazol-3-yl]phenyl}methanesulfonamide (7977303); compound **4**: N^1-cyclopropyl-N^2-(4-methoxyphenyl)-N^2-[(4- methylphenyl)sulfonyl]glycinamide (6382507); compound **5**: *N*-{3-[1-acetyl-5-(2-thienyl)-4,5-dihydro-1*H*-pyrazol-3-yl]phenyl}ethanesulfonamide (7909542); compound **6**: 3-hydroxy-5-(4-methoxyphenyl)-1-(1,3,4-thiadiazol-2-yl)-4-(2-thienylcarbonyl)-1,5-dihydro-2*H*-pyrrol-2-one (6237842); compound **7**: 5-(4-fluorophenyl)-3-hydroxy-4-(5-methyl-2-furoyl)-1-(3-pyridinylmethyl)-1,5-dihydro-2*H*-pyrrol-2-one (6771097); compound **8**: N^1-cyclopropyl-N^2-[(4-methoxyphenyl)sulfonyl]-N^2-(4-methylphenyl)glycinamide (6699002); compound **9**: N^1-cyclopentyl-N^2-(3-methoxyphenyl)-N^2-(phenylsulfonyl)glycinamide (6187162); and compound **10**: 4-({[5-(2-furyl)-4-phenyl-4*H*-1,2,4-triazol-3-yl]thio}methyl)-1,3-thiazol-2-amine (9012750) were purchased from ChemBridge Corporation (San Diego, CA).

4.6. Enzymatic assay

UCH-L3 activity was assayed using modification of a technique described in previous studies.[22,30] The enzyme

reactions were carried out at a final volume of 205 μl on Costar 96-well black assay plates (part number 3915, Corning Inc., Corning, NY). Then, 5 μl of solution containing each compound (100% DMSO), or 5 μl of 100% DMSO as a negative control, was added to 100 μl of enzyme buffer solution (50 pM of UCH-L3, 20 mM Hepes [pH 7.8], 0.5 mM EDTA, 5 mM dithiothreitol [DTT], and 0.1 mg/ml ovalbumin) in each well. The solution was incubated for 30 min at room temperature. To start the enzyme reaction, 100 μl of substrate buffer solution (82 nM of ubiquitin-AMC, 20 mM Hepes [pH 7.8], 0.5 mM EDTA, 5 mM DTT, and 0.1 mg/ml ovalbumin) was added to each well. AMC fluorescence (excitation wavelength: 355 nm, emission wavelength: 460 nm) was subsequently measured 40 times every 3 s with a Wallac 1420 multi-label counter (Perkin-Elmer, Wellesley, MA).

4.7. K_m determination

Fifty microliters of enzyme buffer solution was added to each plate well. The solution was incubated for 30 min at room temperature. To start the enzyme reaction, 50 μl of substrate buffer solution (23.1, 46.3, 92.5, 185, 370, and 740 nM of ubiquitin-AMC; the concentrations of other components were as described previously) was added to each well. Fluorescence of AMC was measured 40 times every 3 s with the Wallac multi-label counter. Initial velocities (from 0 to 30 s) were used for K_m determination, using GraphPad Prism 4 software.[29]

4.8. Experimental IC_{50} determination

Five microliters of solution containing each compound (0.412 μM, 1.23, 3.70, 11.1, 20, 33.3, 50, 100, 300, and 700–850 μM) or 5 μl of 100% DMSO (as a negative control) diluted in 100 μl of enzyme buffer solution was added to each plate well. This solution was incubated for 30 min at room temperature. To start the enzyme reaction, 100 μl of substrate buffer solution was added to each well. Fluorescence of AMC was measured 40 times every 3 s with the Wallac multi-label counter. Initial velocities (from 0 to 30 s) were used for IC_{50} determination, using GraphPad Prism 4 software.[29]

4.9. Active site binding experiment

Modification of a technique described in previous studies was used to determine whether or not the compounds bind to the active site.[22] Five microliters of solution containing compound **1** (0 μM, 61.8 μM, 185 μM, 556 μM, and 1.67 mM) or 5 μl of 100% DMSO (as a negative control) diluted in 80 μl of enzyme buffer solution (UCH-L3: 1 nM) was added to each plate well. This solution was incubated for 30 min at room temperature. To start the enzyme reaction, 80 μl of substrate buffer solution (Ub-AMC: 1 μM) was added to each well, followed within 2 s by addition of 40 μl of iodoacetamide (108 mM) or water as a negative control. Fluorescence of AMC was measured 100 times every second using the Wallac multi-label counter. The percentage of active site survival $[(F_{saturated} - F_t)/(F_{saturated} - F_{t=0}) \times 100]$ was calculated.

Acknowledgments

This work was supported by Grants-in-Aid for Scientific Research from the Ministry of Health, Labour and Welfare of Japan, Grants-in-Aid for Scientific Research from the Ministry of Education, Culture, Sports, Science and Technology of Japan, a grant from the Program for Promotion of Fundamental Studies in Health Sciences of the National Institute of Biomedical Innovation, a grant from Japan Science and Technology Cooperation, and a grant from New Energy and Industrial Technology Development Organization. We thank Takashi Kaburagi for demonstrating how to set up the DOCK software.

References and notes

1. Ciechanover, A.; Schwartz, A. L. *Proc. Natl. Acad. Sci. U.S.A.* **1998**, *95*, 2727–2730.
2. Pickart, C. M.; Rose, I. A. *J. Biol. Chem.* **1985**, *260*, 7903–7910.
3. Waldmeier, P.; Bozyczko-Coyne, D.; Williams, M.; Vaught, J. L. *Biochem. Pharmacol.* **2006**, *72*, 1197–1206.
4. Aktas, O.; Waiczies, S.; Zipp, F. *J. Neuroimmunol.* **2007**, *184*, 17–26.
5. Miyoshi, Y.; Nakayama, S.; Torikoshi, Y.; Tanaka, S.; Ishihara, H.; Taguchi, T.; Tamaki, Y.; Noguchi, S. *Cancer Sci.* **2006**, *97*, 523–529.
6. Rolen, U.; Kobzeva, V.; Gasparjan, N.; Ovaa, H.; Winberg, G.; Kisseljov, F.; Masucci, M. G. *Mol. Carcinog.* **2006**, *45*, 260–269.
7. Kwon, J.; Wang, Y. L.; Setsuie, R.; Sekiguchi, S.; Sato, Y.; Sakurai, M.; Noda, M.; Aoki, S.; Yoshikawa, Y.; Wada, K. *Am. J. Pathol.* **2004**, *165*, 1367–1374.
8. Sano, Y.; Furuta, A.; Setsuie, R.; Kikuchi, H.; Wang, Y. L.; Sakurai, M.; Kwon, J.; Noda, M.; Wada, K. *Am. J. Pathol.* **2006**, *169*, 132–141.
9. Kuntz, I. D.; Blaney, J. M.; Oatley, S. J.; Langridge, R.; Ferrin, T. E. *J. Mol. Biol.* **1982**, *161*, 269–288.
10. Ewing, T. J.; Makino, S.; Skillman, A. G.; Kuntz, I. D. *J. Comput. Aided Mol. Des.* **2001**, *15*, 411–428.
11. FlexX, BioSolveIT GmbH, Sankt Augustin, Germany, <http://www.biosolveit.de/>.
12. Peng, H.; Huang, N.; Qi, J.; Xie, P.; Xu, C.; Wang, J.; Yang, C. *Bioorg. Med. Chem. Lett.* **2003**, *13*, 3693–3699.
13. McNally, V. A.; Gbaj, A.; Douglas, K. T.; Stratford, I. J.; Jaffar, M.; Freeman, S.; Bryce, R. A. *Bioorg. Med. Chem. Lett.* **2003**, *13*, 3705–3709.
14. Olsen, L.; Jost, S.; Adolph, H. W.; Pettersson, I.; Hemmingsen, L.; Jorgensen, F. S. *Bioorg. Med. Chem.* **2006**, *14*, 2627–2635.
15. Miteva, M. A.; Lee, W. H.; Montes, M. O.; Villoutreix, B. O. *J. Med. Chem.* **2005**, *48*, 6012–6022.
16. Johnston, S. C.; Larsen, C. N.; Cook, W. J.; Wilkinson, K. D.; Hill, C. P. *EMBO J.* **1997**, *16*, 3787–3796.
17. Misaghi, S.; Galardy, P. J.; Meester, W. J.; Ovaa, H.; Ploegh, H. L.; Gaudet, R. *J. Biol. Chem.* **2005**, *280*, 1512–1520.
18. RPBS, Paris, France, <http://bioserv.rpbs.jussieu.fr/RPBS/cgi-bin/Ressource.cgi?chzn_lg=an&chzn_rsrc=Collections/>.
19. GOLD User Guide, 16.2.1, CCDC, Cambridge, UK, <http://www.ccdc.cam.ac.uk/support/documentation/gold/3_1/gold31.pdf/>.
20. Dang, L. C.; Melandri, F. D.; Stein, R. L. *Biochemistry* **1998**, *37*, 1868–1879.

21. Mason, D. E.; Ek, J.; Peters, E. C.; Harris, J. L. *Biochemistry* **2004**, *43*, 6535–6544.
22. Liu, Y.; Lashuel, H. A.; Choi, S.; Xing, X.; Case, A.; Ni, J.; Yeh, L. A.; Cuny, G. D.; Stein, R. L.; Lansbury, P. T., Jr. *Chem. Biol.* **2003**, *10*, 837–846.
23. Stenlund, P.; Frostell-Karlsson, A.; Karlsson, O. P. *Anal. Biochem.* **2006**, *353*, 217–225.
24. Das, C.; Hoang, Q. Q.; Kreinbring, C. A.; Luchansky, S. J.; Meray, R. K.; Ray, S. S.; Lansbury, P. T.; Ringe, D.; Petsko, G. A. *Proc. Natl. Acad. Sci. U.S.A.* **2006**, *103*, 4675–4680.
25. Kurihara, L. J.; Semenova, E.; Levorse, J. M.; Tilghman, S. M. *Mol. Cell. Biol.* **2000**, *20*, 2498–2504.
26. Jones, G.; Willett, P.; Glen, R. C.; Leach, A. R.; Taylor, R. *J. Mol. Biol.* **1997**, *267*, 727–748.
27. Hendlich, M.; Rippmann, F.; Barnickel, G. *J. Mol. Graph. Model.* **1997**, *15*, 359–363.
28. Silver, CCDC, Cambridge, UK, <http://www.ccdc.cam.ac.uk/>.
29. GraphPad Prism 4, GraphPad Software, San Diego, CA, <http://www.graphpad.com/www/about.htm/>.
30. Nishikawa, K.; Li, H.; Kawamura, R.; Osaka, H.; Wang, Y. L.; Hara, Y.; Hirokawa, T.; Manago, Y.; Amano, T.; Noda, M.; Aoki, S.; Wada, K. *Biochem. Biophys. Res. Commun.* **2003**, *304*, 176–183.

Available online at www.sciencedirect.com
ScienceDirect
Neuroscience Research 60 (2008) 106–113
Neuroscience Research
www.elsevier.com/locate/neures

Preventing effects of a novel anti-parkinsonian agent zonisamide on dopamine quinone formation

Masato Asanuma [a,*], Ikuko Miyazaki [a], Francisco J. Diaz-Corrales [a], Ko Miyoshi [a], Norio Ogawa [a], Miho Murata [b]

[a] *Department of Brain Science, Okayama University Graduate School of Medicine, Dentistry and Pharmaceutical Sciences, 2-5-1 Shikatacho, Okayama 700-8558, Japan*

[b] *Department of Neurology, Musashi Hospital, National Center of Neurology and Psychiatry, Tokyo, Japan*

Received 10 August 2007; accepted 3 October 2007
Available online 10 October 2007

Abstract

The neurotoxicity of dopamine (DA) quinones as dopaminergic neuron-specific oxidative stress is considered to play a role in the pathogenesis and/or progression of Parkinson's disease (PD), since DA quinones conjugate with several key PD pathogenic molecules (*e.g.*, tyrosine hydroxylase, α-synuclein and parkin) to form protein-bound quinone (quinoprotein) and consequently inhibit their functions. Zonisamide (ZNS) is used as an anti-epileptic agent but also improved the cardinal symptoms of PD in recent clinical trials in Japan. To evaluate the effects of ZNS on excess cytosolic free DA-induced quinone toxicity, we examined changes in DA quinone-related indices after ZNS treatment both in *in vitro* cell-free system and in cultured cells. Co-incubation of DA and ZNS in a cell-free system caused conversion of DA to stable melanin via formation of DA-semiquinone radicals and DA chrome. Long-term (5 days) treatment with ZNS decreased quinoprotein and increased DA/DOPA chromes in dopaminergic CATH.a cells. ZNS significantly inhibited quinoprotein formation induced by treatment with tetrahydrobiopterin and ketanserin that elevate cytosolic free DA in the cells. Our results suggest that the novel anti-parkinsonian agent ZNS possesses preventing effects against DA quinone formation induced by excess amount of cytosolic DA outside the synaptic vesicles.

Keywords: Zonisamide; Dopamine chrome; Dopamine quinone; Quinoprotein; Parkinson's disease

1. Introduction

Under normal conditions, dopamine (DA) is stable in the synaptic vesicle. However, when levodopa is administered to the damaged dopaminergic neuronal system of Parkinson's disease (PD), a large amount of DA remains in the cytosol outside the synaptic vesicle, since the damaged dopaminergic system has too small DA pool to store DA (Sulzer et al., 2000; Sulzer and Zecca, 2000; Asanuma et al., 2003; Ogawa et al., 2005). The toxicity of excess levodopa and/or DA has been well documented in many *in vitro* and *in vivo* animal studies using parkinsonian models (Ogawa et al., 1993; Basma et al., 1995; Walkinshaw and Waters, 1995; Hastings et al., 1996; Asanuma et al., 2003), despite its marked beneficial effects. Free excess DA is easily metabolized via monoamine oxidase (MAO)-B or by auto-oxidation to produce cytotoxic reactive oxygen species (ROS), and then forms neuromelanin (Sulzer et al., 2000; Sulzer and Zecca, 2000). In the oxidation of DA by MAO, DA is converted to dihydroxyphenylacetic acid (DOPAC) to generate general ROS hydrogen peroxide. On the other hand, non-enzymatic and spontaneous auto-oxidation of DA and L-DOPA produces superoxide and reactive quinones such as DA quinones and DOPA quinones (Tse et al., 1976; Graham, 1978). DA quinones are also generated in the enzymatic oxidation of DA by prostaglandin H synthase (cyclooxygenase-2), lipoxygenase, tyrosinase and xanthine oxidase (Korytowski et al., 1987; Rosei et al., 1994; Hastings, 1995; Foppoli et al., 1997; Chae et al., 2007). These quinones are oxidized to the cyclized aminochromes: DA chrome (aminochrome) and DOPA chrome, and then are finally polymerized to form melanin. Although ROS generation by the auto-oxidation of DA may explain widespread

* Corresponding author. Tel.: +81 86 235 7408; fax: +81 86 235 7412.
E-mail address: asachan@cc.okayama-u.ac.jp (M. Asanuma).

0168-0102/$ – see front matter
doi:10.1016/j.neures.2007.10.002

toxicity but not specific damage of DA neurons, the highly reactive DA quinone or DOPA quinone itself exerts predominant cytotoxicity in DA neurons and surrounding neural cells, since these quinones are generated from free cytosolic DA outside the synaptic vesicle or from L-DOPA (Sulzer et al., 2000).

The generated DA quinones covalently conjugate with the sulfhydryl group of cysteine on functional proteins, resulting predominantly in the formation of 5-cysteinyl-DA (Graham, 1978; Fornstedt et al., 1986). DA quinones conjugate with cysteine residues of various functional proteins including several key molecules involved in the pathogenesis of PD (*e.g.*, tyrosine hydroxylase, DA transporter and parkin) to form protein-bound quinones (quinoproteins), and inhibit the function of these proteins to cause DA neuron-specific cytotoxicity (Xu et al., 1998; Kuhn et al., 1999; Whitehead et al., 2001; LaVoie et al., 2005; Machida et al., 2005). We reported previously that repeated levodopa administration elevated striatal DA turnover and formation of quinoproteins specifically in the parkinsonian side, but not in the control side, of hemi-parkinsonian models (Ogawa et al., 2000; Asanuma et al., 2005; Miyazaki et al., 2005). Therefore, the excess amount of cytosolic DA outside the synaptic vesicles after levodopa treatment may exert neurodegenerative effects through quinone generation, at least in the damaged dopaminergic nerve terminals. The DA-induced formation of DA quinones and the consequent dopaminergic cell damage *in vitro* and *in vivo* could be prevented by treatment with superoxide dismutase, glutathione, and certain thiol reagents through their quinone-quenching activities (Offen et al., 1996; Lai and Yu, 1997; Kuhn et al., 1999; Haque et al., 2003). We also demonstrated recently that DA agonists pergolide and pramipexole exhibit quenching properties against *in vitro* generated DA-semiquinone radicals (Asanuma et al., 2005; Miyazaki et al., 2005), and that pergolide effectively prevented repeated levodopa-induced elevation of striatal quinoprotein specifically in parkinsonian models (Miyazaki et al., 2005). Thus, DA quinones act as neurotoxic compounds by eliciting dopaminergic neuron-specific oxidative stress and thus play a role in the pathogenesis and/or progression of PD and neurotoxin-induced parkinsonism (Choi et al., 2003, 2005; Asanuma et al., 2004; LaVoie et al., 2005; Machida et al., 2005; Ogawa et al., 2005; Chae et al., 2007).

Zonisamide (1,2-benzisoxazole-3-methaesulfonamide: ZNS), which was originally synthesized in Japan, has been used as an anti-epileptic agent in Japan, South Korea, USA and Europe. An open trial of ZNS (50–200 mg/day) administered in conjunction with anti-PD drugs showed lessening of symptoms, especially wearing-off (Murata et al., 2001), and induced more than 30% improvement of UPDRS total score up to 3 years (Murata, 2004). The addition of ZNS to levodopa treatment of patients experiencing 'wearing-off' fluctuations resulted in lessening of motor fluctuation and significant improvement of the duration, severity and activities of daily living in 'off' time and score of motor examination. Furthermore, a recent nationwide double-blind controlled study in Japan reported that an adjunctive treatment with lower dose of ZNS (25–100 mg/day) to levodopa improved all the cardinal symptoms of PD (Murata, 2004; Murata et al., 2007).

Several pharmacological effects of ZNS have been proposed to be related to its beneficial effects on PD. ZNS is a specific T-type Ca^{++} channel blocker (Suzuki et al., 1992; Kito et al., 1996), which increases burst firing of dopaminergic neurons in the substantia nigra. A single dose of ZNS increased intracellular and extracellular DOPA, DA and homovanillic acid (HVA) levels and decreased DOPAC level in the rat striatum presumably through its moderate MAO-inhibiting effect (Okada et al., 1992, 1995). Long-term administration of ZNS increased activity and protein level of tyrosine hydroxylase in the rat striatum (Murata, 2004), and thus enhanced DA synthesis. However, these effects cannot fully explain the mechanism of its therapeutic effects on levodopa-induced adverse effects.

To evaluate the effects of ZNS on excess cytosolic free DA-induced quinone toxicity, we examined changes in DA quinone-related indices after ZNS treatment both in *in vitro* cell-free DA-semiquinone generating system and in cultured dopaminergic neuronal cells.

2. Materials and methods

2.1. Materials

DA hydrochloride and L-DOPA were purchased from Wako Pure Chemical (Tokyo, Japan) and Sigma (St. Louis, MO), respectively. ZNS and its sodium salt were provided by Dainippon Sumitomo Pharma (Osaka, Japan).

2.2. ESR spectrometry of generated DA-semiquinone radicals

The spectra of semiquinone radicals generated from DA in a cell-free system were recorded with an electron spin resonance (ESR) spectrometer (JES-FR30, JEOL Co., Tokyo) using a flat quartz cuvette as reported previously (Korytowski et al., 1987; Haque et al., 2003). DA or L-DOPA was dissolved in 10 mM sodium phosphate buffer (PB: pH 7.4), and the pH was adjusted to 7.0 by adding 0.1 M NaOH at 4 °C. For the experiment on time-dependency, the pH-adjusted DA or L-DOPA (final concentration 1 mM) was immediately incubated with ZNS sodium salt dissolved in 10 mM PB (final concentration 8 mM, pH 10.8) for 1–60 min at 37 °C, and the spectra for these combinations were analyzed. As a positive control to generate DA-semiquinone, tyrosinase (final concentration 12.5 μg/ml) was incubated instead of ZNS. Furthermore, 0.1 N NaOH (pH 10.9) or pH-adjusted 10 mM PB (pH 10.8) was used instead of ZNS as a negative control. For the experiment on dose-dependency, the pH-adjusted DA (final concentration 1 mM, pH 7.0), with or without various concentrations (ranging from 2 to 8 mM) of ZNS sodium salt dissolved in 10 mM PB (pH 10.8), was immediately incubated for 1 min at 37 °C, and the spectra for these combinations were analyzed. The pH of each final incubation mixture was approximately 8.0. The signal intensity was evaluated by the relative peak height of the second signal of the semiquinone radical spin adduct (the peak height of the second signal is higher than the others and is directly proportional to double integration of the spectra) to the intensity of the Mn^{2+} signal, which was used as the internal standard to correct for measurement error. The conditions of the ESR spectrometer to estimate the semiquinone radical, including magnetic field, power, modulation frequency, modulation amplitude, response time, temperature, amplitude, and sweep time were 335 ± 5 mT, 4 mW, 9.41 GHz, 79 μT, 0.1 s, 25 °C, 1 × 1000 and 1 min, respectively. Furthermore, the levels of DA and its metabolites in the reaction mixture were measured by high-performance liquid chromatography (HPLC) as described previously (Ogawa et al., 2000; Asanuma et al., 2005).

2.3. Effects of ZNS on generation of DA chrome

To examine the effects of ZNS on generation of DA chrome in a cell-free system, pH-adjusted 1 mM DA in 10 mM PB (pH 6.8) and 0.2% Triton X-100 solution were incubated with or without 200 μM ZNS dissolved in 10 mM PB (pH 6.8) for 1 min to 3 h at 37 °C. The level of DA chrome in the final mixture (pH 6.8) was estimated by measuring absorbance of incubation mixture at 475 nm.

2.4. Cell culture and drug treatment

Dopaminergic CATH.a cells (ATCC; #CRL-11179), derived from mouse DA-containing neurons, were cultured at 37 °C in 5% CO_2 in RPMI 1640 culture medium (Invitrogen, San Diego, CA) supplemented with 4% fetal bovine serum, 8% horse serum, 100 U/ml penicillin and 100 μg/ml streptomycin. Cells were seeded in 6-well plates (Becton Dickinson Labware, Franklin Lakes, NJ) for the extraction of cell lysates used for the measurement of protein-bound quinone and DA/DOPA chrome at a density of 1.0×10^5 cells/cm^2. After 24 h, CATH.a cells were exposed to 1–100 μM ZNS diluted in phosphate buffered saline (PBS) for 5 days for the measurements of quinoprotein and DA/DOPA chrome. To examine the effects of ZNS on excess cytosolic free DA-induced quinone elevation, CATH.a cells were exposed simultaneously to 1–100 μM ZNS with 100 μM tetrahydrobiopterin (BH_4) and 10 μM ketanserin, which enhance DA synthesis and blocks vesicle monoamine transporter, respectively (Choi et al., 2005), for 3 h before extraction of total cell lysates for quinoprotein measurement.

2.5. Protein-bound quinone; quinoprotein measurement

Total cell lysates from drug-treated CATH.a cells were prepared with 10 μg/ml phenylmethylsulfonyl fluoride (Sigma) in ice cold-RIPA buffer [PBS (pH 7.4), 1% nonidet P-40 (NP-40), 0.5% sodium deoxycholate and 0.1% sodium dodecyl sulfate]. The nitrobluetetrazolium (NBT)/glycinate colorimetric assay was performed to detect protein-bound quinones (quinoprotein) (Paz et al., 1991). The cell lysate was added to 500 μl of NBT reagent (0.24 mM NBT in 2 M potassium glycinate, pH 10.0) followed by incubation in the dark for 2 h under constant shaking. The absorbance of blue-purple color developed in the reaction mixture was measured at 530 nm.

2.6. Measurement of DA/DOPA chrome in CATH.a cells

For the measurement of DA/DOPA chrome, cells were solubilized in 500 μl of 1% Triton X-100 solution for 2 h and then centrifuged at 20,000 × *g* for 30 min at 4 °C. The supernatant was used as cell extract and incubated for 3 min at room temperature. The level of DA/DOPA chrome was calculated by measuring absorbance of incubated cell extract at 475 nm. Absorbance values in the *in vitro* incubation of DA (0–500 μM) with tyrosinase (10 μg/ml) for 30 min were used as a standard to calculate the concentration of DA/DOPA chrome in the cell extract.

2.7. Protein measurement

The protein concentration was determined using the Bio-Rad protein assay kit or Bio-Rad DC protein assay kit (Bio-Rad, Richmond, CA), based on the method of Bradford and Lowry, respectively, using bovine serum albumin as a standard.

2.8. Statistical analysis

Results are expressed as mean ± S.E.M. values. Statistical analysis of the data was performed using one-way ANOVA followed by *post hoc* Fisher's PLSD test. A *p*-value less than 0.05 denoted the presence of a statistically significant difference.

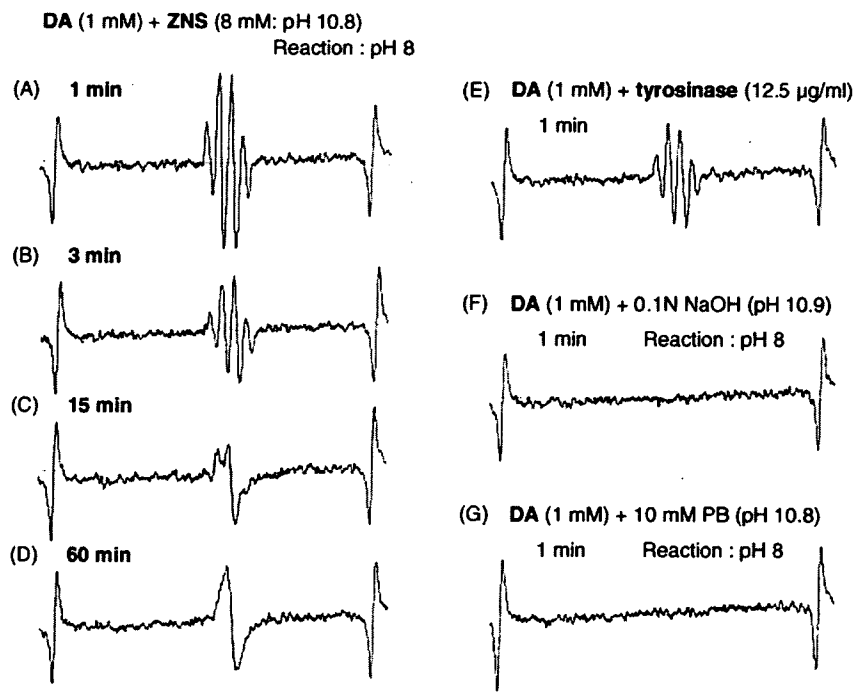

Fig. 1. Effects of ZNS on DA-semiquinone radicals generated from DA in a cell-free system. (A–D) Representative time-course changes in ESR spectra of DA-semiquinone radicals (A–B) to melanin (D) in the incubation of pH-adjusted 1 mM DA (pH 7.0) with 8 mM ZNS (sodium salt) in 10 mM PB (pH 10.8) for 1–60 min at 37 °C at pH 8.0 (incubation mixture). (E) Formation of DA-semiquinone radicals via tyrosinase (12.5 μg/ml)-catalyzed oxidation of 1 mM DA. (F and G) No signals for radical formation at pH 8.0 (incubation mixture) when pH-adjusted 1 mM DA (pH 7.0) was incubated for 1 min at 37 °C with 0.1 N NaOH (pH 10.9) (F) or pH-adjusted 10 mM PB (pH 10.8) (G). Each experiment was performed as triplicate assays.

3. Results

3.1. Effects of ZNS on generated DA-semiquinone radicals in a cell-free system

When a high dose of DA (5 mM) was incubated at 37 °C at neutral pH 7–8, the formation of DA-semiquinone radicals started immediately within 1 min, peaked at around 1 min, then gradually decreased and continued for 10 min, as shown in a previous study (Haque et al., 2003). In the present ESR study, however, no signals for radical formation were detected at pH 8 (incubation mixture) when a lower dose of pH-adjusted 1 mM DA (pH 7.0) was incubated for 1 min at 37 °C with 0.1 N NaOH (pH 10.9) or pH-adjusted 10 mM PB (pH 10.8) (Fig. 1F and G). Interestingly, when pH-adjusted 1 mM DA (pH 7.0) was incubated at 37 °C with 8 mM ZNS (sodium salt) in 10 mM PB (pH 10.8), the formation of DA-semiquinone radicals, which was identified by four waves in ESR spectrometry, started immediately within 1 min and peaked at around 1 min, at pH 8 (incubation mixture) (Fig. 1A and B), as well as formation of DA-semiquinone radicals via tyrosinase-catalyzed oxidation of DA (Fig. 1E). Then, the DA-semiquinone radical induced by incubation of DA and ZNS converted to melanin, which was recognized by a wide single wave, at 15–60 min (Fig. 1C and D). The incubation of pH-adjusted 1 mM DA (pH 7.0) and 2–8 mM ZNS (sodium salt, pH 10.8) at pH 8 (incubation mixture) resulted in DA-semiquinone radical formation at 1 min (Fig. 2A–D) and subsequent melanin formation at 60 min (data not shown) in a ZNS concentration-dependent manner. Furthermore, incubation of pH-adjusted 1 mM L-DOPA (pH 7.0) with 8 mM ZNS (sodium salt, pH 10.8) at 37 °C at pH 8 (incubation mixture) resulted in immediate generation of DOPA-semiquinone radicals within 1 min, with a peak at around 1 min, and conversion to melanin within up to 20 min (Fig. 2E–G). DOPAC, 3-methoxy tyramine and HVA, which are metabolites of DA via MAO and/or catecholamine *o*-methyltransferase, were not detected in any incubation mixture of pH-adjusted DA and ZNS (sodium salt) at either dose of ZNS or incubation time by HPLC (data not shown).

3.2. Effects of ZNS on generation of DA chrome in a cell-free system

Because a high dose of ZNS was required to detect the conversion effects from DA to melanin in ESR spectrometry, we used sodium salt of ZNS, which is highly soluble in 10 mM PB, at a dose of 2–8 mM. However, the pH value of the mixture of ESR examination was slightly alkaline at 8.0 because of high alkalinity of ZNS sodium salt solution (pH 10.8) in the cell-free system. To examine the effects of relatively low dose of ZNS on conversion of DA to melanin at neutral pH, we evaluated generation of DA chrome, which is an intermediate in conversion of DA quinone to melanin, using 200 μM ZNS at pH 6.8, but not its sodium salt (Fig. 3). Although the incubation of pH-adjusted 1 mM DA (pH 6.8) alone at 37 °C showed time-dependent but not significant increases in DA

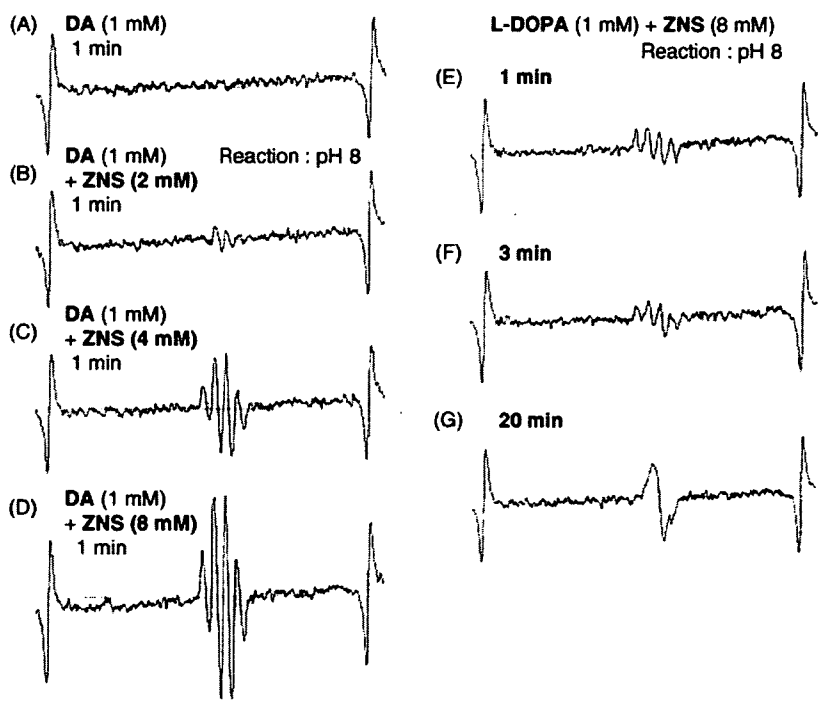

Fig. 2. Effects of ZNS on semiquinone radicals generated from DA or L-DOPA. (A–D) Dose-dependent effects of ZNS on DA-semiquinone radicals generated from DA in a cell-free system. The pH-adjusted 1 mM DA (pH 7.0) was simultaneously incubated with 2–8 mM ZNS (pH 10.8) at pH 8.0 (incubation mixture) for 1 min at 37 °C, and then the relative signal intensity of DA-semiquinone radicals was measured by ESR spectrometry. (E–G) Representative time-course changes in ESR spectra of DOPA-semiquinone radicals (E and F) to melanin (G) in the incubation of pH-adjusted L-DOPA (1 mM, pH 7.0) with 8 mM ZNS (sodium salt) in 10 mM PB (pH 10.8) for 1–20 min at 37 °C at pH 8.0 (incubation mixture). Three independent assays were performed in each experiment.

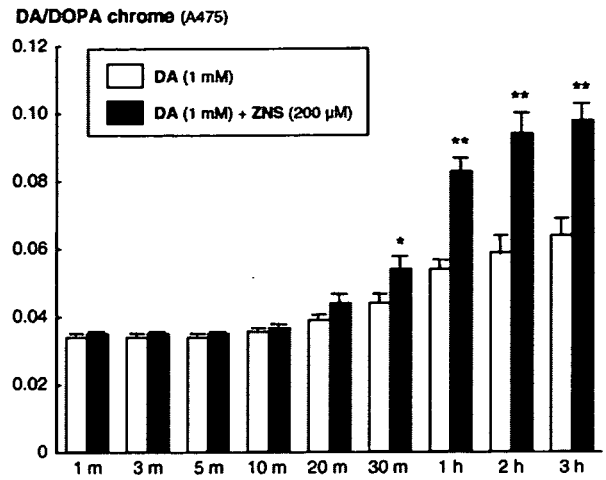

Fig. 3. Effects of ZNS on time-course changes in DA/DOPA chrome generated in a cell-free system. Levels of generated DA/DOPA chrome were measured after incubation of pH-adjusted 1 mM DA (pH 6.8) with/without 200 μM ZNS (pH 6.8) at 37 °C for 1 min to 3 h. Co-incubation of pH-adjusted DA (1 mM) and ZNS (200 μM) at neutral pH significantly increased DA/DOPA chrome at 30 min to 3 h, compared with time-matched pH-adjusted DA alone. Each value is the mean of absorbance at 475 nm ± S.E.M. ($n = 5$). *$p < 0.05$, **$p < 0.001$ compared with time-matched group treated with DA alone.

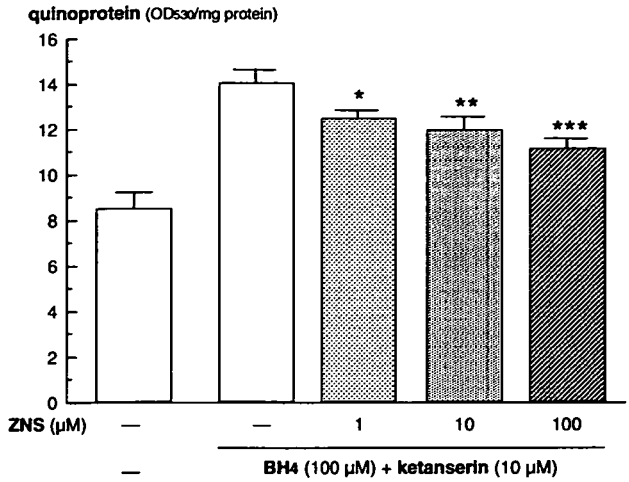

Fig. 5. Effects of ZNS treatment on excess cytosolic free DA-induced quinoprotein formation in dopaminergic CATH.a cells. Quinoprotein level in CATH.a cells were measured after treatment with BH_4 (100 μM) and ketanserin (10 μM), with or without ZNS (1–100 μM) for 3 h. The simultaneous treatment of ZNS (1–100 μM) significantly and dose-dependently inhibited BH_4 plus ketanserin-induced quinoprotein formation. Data are mean ± S.E.M. ($n = 8$). *$p < 0.05$, **$p < 0.01$ and ***$p < 0.001$ compared with cells treated with BH_4 plus ketanserin without ZNS.

chrome level, co-incubation of pH-adjusted 1 mM DA (pH 6.8) and 200 μM ZNS (pH 6.8) at 37 °C significantly increased DA chrome at 30 min to 3 h, compared with time-matched pH-adjusted DA alone.

3.3. Effects of ZNS on DA quinone formation in CATH.a cells

We examined changes in DA, its metabolites, quinoprotein and DA/DOPA chrome using *in vitro* dopaminergic CATH.a cells after 5-day treatment of ZNS. Quinoprotein level was significantly decreased after 5-day treatment of ZNS (10–100 μM) (Fig. 4) with reduction of DOPAC level (data not shown). On the other hand, 5-day treatment of ZNS (1–100 μM) significantly increased DA/DOPA chrome level in CATH.a cells (Fig. 4).

Finally, we examined the effects of ZNS on excess cytosolic free DA-induced quinone formation by measuring quinoprotein levels in CATH.a cells after treatment with BH_4 (100 μM) and ketanserin (10 μM) with/without ZNS (1–100 μM) for 3 h. The quinoprotein levels in CATH.a cells co-treated with BH_4 and ketanserin for 3 h (which increase cytosolic free DA) were relatively higher than that in control at day 1 (Fig. 5), in agreement with a previous report (Choi et al., 2005). The simultaneous treatment of ZNS (1–100 μM) significantly and dose-dependently inhibited BH_4- and ketanserin-induced quinoprotein formation in the cells (Fig. 5).

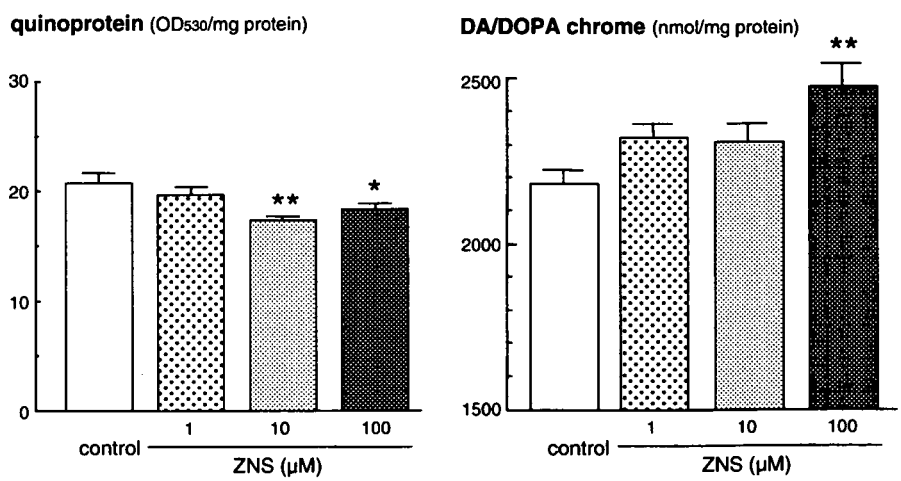

Fig. 4. Effects of long-term treatment of ZNS on quinoprotein and DA/DOPA chrome in dopaminergic CATH.a cells. After treatment with ZNS (1–100 μM) for 5 days, levels of quinoprotein ($n = 5$) and DA/DOPA chrome ($n = 6$) were measured in dopaminergic CATH.a cells, as indicated in Section 2. Data are mean ± S.E.M. *$p < 0.05$, **$p < 0.01$ compared with the control group.

4. Discussion

The main findings of this study are: (1) co-incubation of DA and ZNS in a cell-free system caused conversion of DA to stable melanin via formation of DA-semiquinone radicals and DA chrome; (2) long-term treatment with ZNS for 5 days decreased quinoprotein and increased DA/DOPA chromes in dopaminergic CATH.a cells; and (3) ZNS significantly inhibited quinoprotein formation induced by BH_4 and ketanserin that increase cytosolic free DA in the cells.

Long-term treatment of patients with PD by levodopa frequently causes various adverse effects including the wearing-off phenomenon, dyskinesia and psychiatric symptoms (Ahlskog and Muenter, 2001; Ogawa et al., 2005). However, long-term levodopa treatment-induced adverse effects that might be based on permanent neuronal network remodeling were seen specifically in PD patients but not in normal subjects or neurological diseases other than PD (Ogawa et al., 2005). Since the striatal damaged nerve terminal have too small DA pool to store DA at advanced stage of PD, repeated intermittent pulsatile levodopa stimulation results in free DA excess in the cytosol outside the synaptic vesicle (Sulzer et al., 2000; Sulzer and Zecca, 2000; Asanuma et al., 2003; Ogawa et al., 2005). The previous study revealed that repeated levodopa administration elevated striatal quinoprotein levels specifically on the parkinsonian side, not on the control side, of hemi-parkinsonian mice (Miyazaki et al., 2005). Therefore, the parkinsonian side-specific elevation of quinone generation may be due to excess amount of cytosolic DA outside the synaptic vesicles, which is easily oxidized to DA quinones in damaged dopaminergic nerve terminals after repeated levodopa treatment. In cultured dopaminergic cells, simultaneous treatment with ZNS dose-dependently suppressed BH_4- and ketanserin-induced quinoprotein formation via elevation of cytosolic free DA (Fig. 5), suggesting that ZNS has potent neuroprotective effects against neurotoxicity of DA quinone induced by excess amount of cytosolic DA outside the synaptic vesicles.

The protective effects of ZNS against levodopa-induced DA quinone toxicity in parkinsonian models may be based, in part, on its stabilizing effects against free DA and cytotoxic DA quinone; ZNS can convert free DA to melanin via the formation of DA-semiquinone radicals (Figs. 1 and 2) and subsequent intermediate DA chrome in the cell-free system (Fig. 3). This possible mechanism is also supported by the present results of long-term treatment with ZNS in cultured dopaminergic CATH.a cells. Long-term ZNS treatment in CATH.a cells for 5 days significantly decreased quinoprotein and increased DA/DOPA chromes (Fig. 4) with reduction of DOPAC (data not shown), suggesting that continuous ZNS exposure to DA-rich CATH.a cells promotes conversion of free DA and DA quinone to DA chrome, then to melanin. However, these effects do not seem to be exerted in a dose-dependent manner. Likewise relatively low doses of ZNS (25, 50 mg/day) rather than 100 mg/day significantly improved UPDRS Part III total score in the clinical trial (Murata et al., 2007), there may be optimal concentration range of ZNS to exert its stabilizing effects against DA quinones.

Several neuroprotective strategies have been proposed against DA quinone-induced cytotoxicity: (1) quenching excess free DA and DA quinone, (2) inhibiting quinone formation, and (3) enhancing intrinsic antioxidative system against DA quinone toxicity (Asanuma et al., 2004). Regarding quenching DA quinone, DA quinone can be scavenged by direct conjugation with some drugs, *e.g.*, thiol-containing compounds (*N*-acetylcyteine and dithiothreitol) (Offen et al., 1996) and DA agonists (pergolide and pramipexole) (Asanuma et al., 2005; Miyazaki et al., 2005). Furthermore, another possible method to quench DA quinone-induced cytotoxicity is the conversion of free DA and DA quinone to stable melanin. The final oxidized form of DA quinone, neuromelanin, exerts cytoprotective effects through its binding capacity to toxic metals (Zecca et al., 2003). Although large amount of neuromelanin with iron is reported to be potentially cytotoxic, physiological amount of neuromelanin is not toxic and rather cytoprotective with its high storage capacity for toxic metals in the substantia nigra (Gerlach et al., 2003; Zecca et al., 2003). This cytoprotective potency by stabilization of DA quinone has been clarified by our previous report that melanin-synthesizing enzyme tyrosinase ameliorates methamphetamine-induced neurotoxicity and quinoprotein formation *in vitro* and *in vivo* by its rapid conversion of DA quinone to melanin (Miyazaki et al., 2006). Also in the present study, we showed that ZNS can convert free DA to melanin via the formation of DA quinone and the intermediate DA chrome in the cell-free system. Therefore, these stabilizing effects of ZNS on free DA and DA quinone by the conversion to melanin may be one of the plausible mechanisms of its prevention against DA quinone-induced cytotoxicity.

ZNS is also known to scavenge hydroxyl radicals and nitric oxide radicals in a cell-free system (Mori et al., 1998) and inhibits lipid peroxidation and oxidative DNA damage in the rat brain (Komatsu et al., 2000). The general ROS such as hydroxyl radicals and nitric oxide radicals show widespread toxicity not only in DA neurons but also in other regions. Since the DA quinone is specifically generated from free cytosolic DA (Sulzer et al., 2000), the stabilizing effects of ZNS on free DA and cytotoxic DA quinone as dopaminergic neuron-specific oxidative stress may play a role in its preventing property against DA or levodopa-induced DA quinone toxicity, in addition to its scavenging activity against general ROS.

In conclusion, ZNS suppressed excess cytosolic free DA-induced quinone generation in dopaminergic cells. Furthermore, ZNS stabilized free DA and DA quinone as dopaminergic neuron-specific oxidative stress by the conversion to melanin. The stabilizing effects of ZNS against cytotoxic DA quinones may play a role in the efficacy of its adjunctive treatment to levodopa in parkinsonian patients.

Acknowledgments

This work was supported in part by Health and Labour Sciences Research Grants for Research on Measures for Intractable Diseases, for Research on Psychiatric and Neuro-

logical Diseases and Mental Health, and for Comprehensive Research on Aging and Health from the Japanese Ministry of Health, Labour and Welfare, and by Grants-in-Aid for Young Scientists (B) and for Scientific Research (C) from the Japanese Ministry of Education, Culture, Sports, Science and Technology. We would like to thank Mr. Yusuke Urakubo, Mr. Yasutsugu Tsutsui, and Mr. Masashi Yoshimoto for their technical assistance.

References

Ahlskog, J.E., Muenter, M.D., 2001. Frequency of levodopa-related dyskinesias and motor fluctuations as estimated from the cumulative literature. Mov. Disord. 16, 448–458.

Asanuma, M., Miyazaki, I., Diaz-Corrales, F.J., Ogawa, N., 2004. Quinone formation as dopaminergic neuron-specific oxidative stress in pathogenesis of sporadic Parkinson's disease and neurotoxin-induced parkinsonism. Acta Med. Okayama 58, 221–233.

Asanuma, M., Miyazaki, I., Diaz-Corrales, F.J., Shimizu, M., Tanaka, K., Ogawa, N., 2005. Pramipexole has ameliorating effects on levodopa-induced abnormal dopamine turnover in parkinsonian striatum and quenching effects on dopamine-semiquinone generated *in vitro*. Neurol. Res. 27, 533–539.

Asanuma, M., Miyazaki, I., Ogawa, N., 2003. Dopamine- or L-DOPA-induced neurotoxicity: the role of dopamine quinone formation and tyrosinase in a model of Parkinson's disease. Neurotox. Res. 5, 165–176.

Basma, A.N., Morris, E.J., Nicklas, W.J., Geller, H.M., 1995. L-dopa cytotoxicity to PC12 cells in culture is via its autoxidation. J. Neurochem. 64, 825–832.

Chae, S.W., Bang, Y.J., Kim, K.M., Lee, K.Y., Kang, B.Y., Kim, E.M., Inoue, H., Hwang, O., Choi, H.J., 2007. Role of cyclooxygenase-2 in tetrahydrobiopterin-induced dopamine oxidation. Biochem. Biophys. Res. Commun. 359, 735–741.

Choi, H.J., Kim, S.W., Lee, S.Y., Hwang, O., 2003. Dopamine-dependent cytotoxicity of tetrahydrobiopterin: a possible mechanism for selective neurodegeneration in Parkinson's disease. J. Neurochem. 86, 143–152.

Choi, H.J., Lee, S.Y., Cho, Y., Hwang, O., 2005. Inhibition of vesicular monoamine transporter enhances vulnerability of dopaminergic cells: relevance to Parkinson's disease. Neurochem. Int. 46, 329–335.

Foppoli, C., Coccia, R., Cini, C., Rosei, M.A., 1997. Catecholamines oxidation by xanthine oxidase. Biochim. Biophys. Acta 1334, 200–206.

Fornstedt, B., Rosengren, E., Carlsson, A., 1986. Occurrence and distribution of 5-*S*-cysteinyl derivatives of dopamine, dopa and dopac in the brains of eight mammalian species. Neuropharmacology 25, 451–454.

Gerlach, M., Double, K.L., Ben-Shachar, D., Zecca, L., Youdim, M.B., Riederer, P., 2003. Neuromelanin and its interaction with iron as a potential risk factor for dopaminergic neurodegeneration underlying Parkinson's disease. Neurotox. Res. 5, 35–44.

Graham, D.G., 1978. Oxidative pathways for catecholamines in the genesis of neuromelanin and cytotoxic quinones. Mol. Pharmacol. 14, 633–643.

Haque, M.E., Asanuma, M., Higashi, Y., Miyazaki, I., Tanaka, K., Ogawa, N., 2003. Apoptosis-inducing neurotoxicity of dopamine and its metabolites via reactive quinone generation in neuroblastoma cells. Biochim. Biophys. Acta 1619, 39–52.

Hastings, T.G., 1995. Enzymatic oxidation of dopamine: the role of prostaglandin H synthase. J. Neurochem. 64, 919–924.

Hastings, T.G., Lewis, D.A., Zigmond, M.J., 1996. Role of oxidation in the neurotoxic effects of intrastriatal dopamine injections. Proc. Natl. Acad. Sci. U.S.A. 93, 1956–1961.

Kito, M., Maehara, M., Watanabe, K., 1996. Mechanisms of T-type calcium channel blockade by zonisamide. Seizure 5, 115–119.

Komatsu, M., Hiramatsu, M., Willmore, L.J., 2000. Zonisamide reduces the increase in 8-hydroxy-2'-deoxyguanosine levels formed during iron-induced epileptogenesis in the brains of rats. Epilepsia 41, 1091–1094.

Korytowski, W., Sarna, T., Kalyanaraman, B., Sealy, R.C., 1987. Tyrosinase-catalyzed oxidation of dopa and related catechol(amine)s: a kinetic electron spin resonance investigation using spin-stabilization and spin label oximetry. Biochim. Biophys. Acta 924, 383–392.

Kuhn, D.M., Arthur Jr., R.E., Thomas, D.M., Elferink, L.A., 1999. Tyrosine hydroxylase is inactivated by catechol-quinones and converted to a redox-cycling quinoprotein: possible relevance to Parkinson's disease. J. Neurochem. 73, 1309–1317.

Lai, C.T., Yu, P.H., 1997. Dopamine- and L-β-3,4-dihydroxyphenylalanine hydrochloride (L-Dopa)-induced cytotoxicity towards catecholaminergic neuroblastoma SH-SY5Y cells. Effects of oxidative stress and antioxidative factors. Biochem. Pharmacol. 53, 363–372.

LaVoie, M.J., Ostaszewski, B.L., Weihofen, A., Schlossmacher, M.G., Selkoe, D.J., 2005. Dopamine covalently modifies and functionally inactivates parkin. Nat. Med. 11, 1214–1221.

Machida, Y., Chiba, T., Takayanagi, A., Tanaka, Y., Asanuma, M., Ogawa, N., Koyama, A., Iwatsubo, T., Ito, S., Jansen, P.H., Shimizu, N., Tanaka, K., Mizuno, Y., Hattori, N., 2005. Common anti-apoptotic roles of parkin and alpha-synuclein in human dopaminergic cells. Biochem. Biophys. Res. Commun. 332, 233–240.

Miyazaki, I., Asanuma, M., Diaz-Corrales, F.J., Fukuda, M., Kitaichi, K., Miyoshi, K., Ogawa, N., 2006. Methamphetamine-induced dopaminergic neurotoxicity is regulated by quinone formation-related molecules. FASEB J. 20, 571–573.

Miyazaki, I., Asanuma, M., Diaz-Corrales, F.J., Miyoshi, K., Ogawa, N., 2005. Dopamine agonist pergolide prevents levodopa-induced quinoprotein formation in parkinsonian striatum and shows quenching effects on dopamine-semiquinone generated *in vitro*. Clin. Neuropharmacol. 28, 155–160.

Mori, A., Noda, Y., Packer, L., 1998. The anticonvulsant zonisamide scavenges free radicals. Epilepsy Res. 30, 153–158.

Murata, M., 2004. Novel therapeutic effects of the anti-convulsant, zonisamide, on Parkinson's disease. Curr. Pharm. Des. 10, 687–693.

Murata, M., et al., 2007. Zonisamide improves motor function in Parkinson disease: a randomized, double-blind study. Neurology 68, 45–50.

Murata, M., Horiuchi, E., Kanazawa, I., 2001. Zonisamide has beneficial effects on Parkinson's disease patients. Neurosci. Res. 41, 397–399.

Offen, D., Ziv, I., Sternin, H., Melamed, E., Hochman, A., 1996. Prevention of dopamine-induced cell death by thiol antioxidants: possible implications for treatment of Parkinson's disease. Exp. Neurol. 141, 32–39.

Ogawa, N., Asanuma, M., Miyazaki, I., Diaz-Corrales, F.J., Miyoshi, K., 2005. L-DOPA treatment from the viewpoint of neuroprotection: possible mechanism of specific and progressive dopaminergic neuronal death in Parkinson's disease. J. Neurol. 252 (Suppl. 4), iv23–iv31.

Ogawa, N., Edamatsu, R., Mizukawa, K., Asanuma, M., Kohno, M., Mori, A., 1993. Degeneration of dopaminergic neurons and free radicals. Possible participation of levodopa. Adv. Neurol. 60, 242–250.

Ogawa, N., Tanaka, K., Asanuma, M., 2000. Bromocriptine markedly suppress levodopa-induced abnormal increase of dopamine turnover in the parkinsonian striatum. Neurochem. Res. 25, 755–758.

Okada, M., Kaneko, S., Hirano, T., Ishida, M., Kondo, T., Otani, K., Fukushima, Y., 1992. Effects of zonisamide on extracellular levels of monoamine and its metabolite, and on Ca^{2+} dependent dopamine release. Epilepsy Res. 13, 113–119.

Okada, M., Kaneko, S., Hirano, T., Mizuno, K., Kondo, T., Otani, K., Fukushima, Y., 1995. Effects of zonisamide on dopaminergic system. Epilepsy Res. 22, 193–205.

Paz, M.A., Fluckiger, R., Boak, A., Kagan, H.M., Gallop, P.M., 1991. Specific detection of quinoproteins by redox-cycling staining. J. Biol. Chem. 266, 689–692.

Rosei, M.A., Blarzino, C., Foppoli, C., Mosca, L., Coccia, R., 1994. Lipoxygenase-catalyzed oxidation of catecholamines. Biochem. Biophys. Res. Commun. 200, 344–350.

Sulzer, D., Bogulavsky, J., Larsen, K.E., Behr, G., Karatekin, E., Kleinman, M.H., Turro, N., Krantz, D., Edwards, R.H., Greene, L.A., Zecca, L., 2000. Neuromelanin biosynthesis is driven by excess cytosolic catecholamines not accumulated by synaptic vesicles. Proc. Natl. Acad. Sci. U.S.A. 97, 11869–11874.

Sulzer, D., Zecca, L., 2000. Intraneuronal dopamine-quinone synthesis: a review. Neurotox. Res. 1, 181–195.

Suzuki, S., Kawakami, K., Nishimura, S., Watanabe, Y., Yagi, K., Seino, M., Miyamoto, K., 1992. Zonisamide blocks T-type calcium channel in cultured neurons of rat cerebral cortex. Epilepsy Res. 12, 21–27.

Tse, D.C., McCreery, R.L., Adams, R.N., 1976. Potential oxidative pathways of brain catecholamines. J. Med. Chem. 19, 37–40.

Walkinshaw, G., Waters, C.M., 1995. Induction of apoptosis in catecholaminergic PC12 cells by L-DOPA. Implications for the treatment of Parkinson's disease. J. Clin. Invest. 95, 2458–2464.

Whitehead, R.E., Ferrer, J.V., Javitch, J.A., Justice, J.B., 2001. Reaction of oxidized dopamine with endogenous cysteine residues in the human dopamine transporter. J. Neurochem. 76, 1242–1251.

Xu, Y., Stokes, A.H., Roskoski Jr., R., Vrana, K.E., 1998. Dopamine, in the presence of tyrosinase, covalently modifies and inactivates tyrosine hydroxylase. J. Neurosci. Res. 54, 691–697.

Zecca, L., Zucca, F.A., Wilms, H., Sulzer, D., 2003. Neuromelanin of the substantia nigra: a neuronal black hole with protective and toxic characteristics. Trends Neurosci. 26, 578–580.